

Frank Elastic Constants of Semiflexible Polymer Solutions

Quinn MacPherson

*Science Division, College of the Sequoias**

(Dated: July 18, 2022)

We derive the Frank elastic constants for nematic solutions of semiflexible polymers. We plot these results as a function of the coarse-grained Maier-Saupe quadrupole aligning strength and polymer stiffness ranging from rigid to highly flexible. The derivation uses the random phase approximation and combines the exact results for the statistics of a worm-like-chain with polymer field theory using a spherical harmonic basis. The results are evaluated using a numerical inverse Laplace transform. We present the results in terms of microscopic features such as hairpins and polymer ends so the trends can be understood independently from the derivation. Key findings are that for rigid polymers $K_{bend} > K_{splay} > K_{twist}$ while for flexible polymers $K_{splay} > K_{bend} > K_{twist}$. For rigid polymers, the Frank elastic constants grow with the polymer length. For flexible polymers the elastic constants grow with the persistence length, which becomes the characteristic length scale, with the exception of K_{splay} at high alignment strengths which grows with polymer lengths due to the elimination of hairpins.

I. INTRODUCTION

When oblong molecules are sufficiently concentrated they tend to align. This liquid crystalline alignment results from the molecules being much easier to pack together when the molecules are oriented in roughly the same direction as their neighbors. That is, the alignment is an entropic effect, though an enthalpic contribution is also possible. Polymers, which are characterised by a length that is much larger than their diameter, are oblong in the extreme. Solutions and melts of semiflexible and rigid polymers are particularly prone to alignment because their structural rigidity tends to align monomers along the polymer backbone, compounding the aligning tendency from packing.

Even for highly packed solutions of rigid polymers, imperfections in the packing will cause the direction of alignment to wander so that distant positions in the solution will have different local directions of alignment. The orientation of alignment is critical to the behavior of polymer solutions ranging from conducting polymers [2] to the packaging of DNA within a viral capsid [3]. The deviations of the local direction of liquid crystal alignment over large distances can be classified into bend, twist, and splay which are depicted in figure 1.

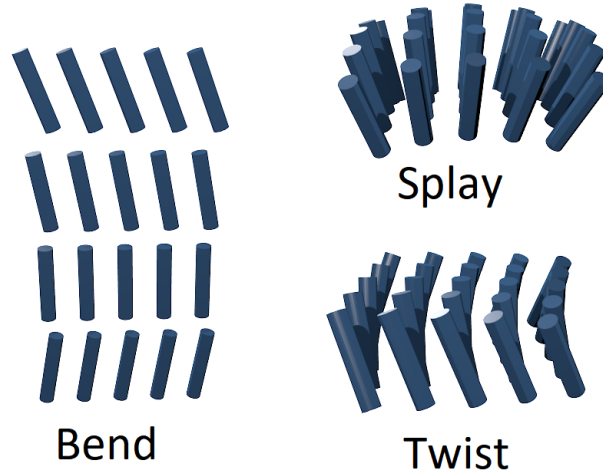


FIG. 1. Pictorial representation of bend, twist, and splay. The axes of the cylinders represent the direction of nematic ordering, \vec{n} . We cite [1] for the format of this figure.

* Previously at Department of Physics, Stanford University.

We formally define bend as $\vec{n} \times \nabla \times \vec{n}$, twist as $\vec{n} \cdot \nabla \times \vec{n}$, and splay as $\nabla \cdot \vec{n}$ where the unit vector \vec{n} denotes the direction of alignment (we will formally define \vec{n} in equation 88). If deviations in the direction of alignment occur slowly – i.e. over large spatial distances – then bend, twist, and splay will be small due the presence of the spatial derivative ∇ . Because these deformations are small, we can write the energy of these deformation modes as a quadratic in bend, twist, and splay

$$E_{Frank} = \frac{1}{2}K_{bend} \left\langle (\vec{n} \times \nabla \times \vec{n})^2 \right\rangle + \frac{1}{2}K_{twist} \left\langle (\vec{n} \cdot \nabla \times \vec{n})^2 \right\rangle + \frac{1}{2}K_{splay} \left\langle (\nabla \cdot \vec{n})^2 \right\rangle \quad (1)$$

where K_{bend} , K_{twist} , and K_{splay} are the Frank elastic constants for the (achiral) solution. In writing Eq. 1, we have included only long distance (small k) terms and hence ignore higher order derivative terms such as the saddle-splay interaction.

The central theme of material science is to predict macroscopic material properties from microstructure, which in turn is generated by the molecular properties of the constituents. Here we consider the latter connection between the molecular properties (in this case, the polymer length, concentration, Kuhn length and monomer cross sectional area) and the microstructure (bend, twist, and splay). We are particularly interested in the large effects that the flexibility or rigidity of the polymer backbone can have on the Frank elastic constants.

The first step to building a theoretic model of the elastic response of a solution is to model the thermodynamics of the solution. In other words, when should we expect the aligned phase to even exist? The phase behavior of solutions of semiflexible polymers have been investigated by a number of authors [4–11]. The interested reader is referred to these references for the resulting phase diagrams. These dictate the minimum possible degree of alignment where a nematic phase can be found.

Another important step is deriving the elastic constants for solutions in the rigid rod limit [12–14]. This is the limiting case for a polymer of infinite Kuhn length, to which we will compare our results. There has also been considerable work on deriving the Frank elastic constants of semiflexible polymer solutions under various approximations and conditions [9, 15–19]. Shimada [16] makes the approximation of a weak aligning field. Petschek and Terentjev [18] estimated Frank elastic constants of a chain of monomers connected by stiff joints using a ground-state-dominance approximation[20]. Santo and Teramoto [19] found the Frank constants for a freely jointed chain and tabulated results of previous papers.

Exact results for the propagator of the wormlike chain in an aligning field were found by Spakowitz and Wong [21, 22] and enable a better determination of polymer statistics. We use this propagator in conjunction with polymer field theory to more accurately determine the Frank elastic constants. While a connection between spherical harmonics and the Frank elastic modes has long been recognized [23], we introduce spherical tensor fields and compact summation notation which simplify and clarify the field theory derivation (see equations 7 and 10). The derivation of the Frank elastic constants we present remains analytical up to an inverse Laplace transform, which we perform numerically. The results and their interpretation, which are intended to be intelligible without reference to the derivation, are presented in section XVII.

II. MODEL AND ASSUMPTIONS

A. Solution of WLC's

We wish to study deformations in the alignment of liquid crystal polymer solutions and melts. To this end we propose the following mathematical model and approximations. The point(s) at which an approximation is used in the subsequent derivation will be noted for those wishing to relax these assumptions.

1. We will assume all polymers have the same length, L , i.e. no polydispersity.
2. We describe the j^{th} polymer as a continuous path in space $\vec{r}_j(s)$, given as a function of path length $s \in [0, L]$. We define the orientation direction of the polymer at point s as the unit vector $\vec{u}_j(s) = \frac{\partial \vec{r}_j(s)}{\partial s}$.
3. Each polymer will be assumed to obey the statistics of an inextensible Worm Like Chain (WLC). That is, the mechanical energy of n_p polymers is given by

$$E_{poly} \equiv \frac{1}{2}\ell_p \sum_{j=1}^{n_p} \int_0^L ds \left(\frac{\partial \vec{u}_j}{\partial s} \right)^2 \quad (2)$$

where ℓ_p is the persistence length of the polymer, which sets the polymer stiffness. In other words, the energy is proportional to the square of the curvature of the polymers. Along with all other energies in this paper, E_{poly} is assumed to be in units of $k_b T$.

4. The cross sectional area of the polymer is sufficiently small that its diameter is smaller than the other length scales of interest in the problem.
5. The polymers are achiral. That is, they do not exhibit a natural twist direction that affects the solution properties. As an example of how this could be violated, imagine a naturally twisted polymer and further imagine that the alignment interactions between adjacent chains depend on this twist, such that a natural twist is conferred to the polymer solution.
6. The system is unchanged by reversing any polymer by swapping its $s = 0$ and $s = L$ ends. An example of how this could be violated would be a solution of polymers with a negative charge on one polymer end and a positive charge on the other. Such polymers would have dipole-dipole interactions and/or experience the aligning effect of an external field.
7. The system is translationally invariant. With no boundary conditions the material can be thought of as being infinite in extent.
8. We will assume the solvent is good enough that the solution does not segregate into a polymer rich and polymer lean phase. The range of applicability of this assumption in the presence of an alignment interaction is studied in [11].
9. Polymer interactions are assumed to be two body interactions, that is, the energy is quadratic in polymer density.
10. Polymer interactions are local, meaning that their range is well below the length scales of relevance to the liquid crystal alignment fluctuation under study.
11. There are only two polymer interactions. The first of these is the Flory-Huggins interaction which governs the energy of mixing of polymer and solvent. The second is a Maier-Saupe interaction which captures the tendency of adjacent polymer segments to align with each other by assigning an energy proportional to $(\vec{u}_1 \cdot \vec{u}_2)^2$ for two polymer segments in close spatial proximity.
12. The preferential direction of alignment is approximately in the z direction. The density and the preferred direction of alignment of the polymers will only make small deviations from their mean field values. Note that the orientation of particular polymers can differ substantially from the z direction.
13. The effective potential experienced by a single polymer, created by the others, undergoes only small fluctuations from its mean value. This allows the Random Phase Approximation (RPA).
14. The average alignment field will be azimuthally symmetric with respect to the aligning axis. In other words, there is not a second axis of alignment that could result from ribbon-like polymers with an asymmetric cross-section.
15. We are primarily interested in coordinated deviations of the alignment over large distances (small \vec{k}).

B. Fuzzball and Rigid Rod

The properties of the WLC are made more evident by comparison to the rigid rod and an object I will refer to as a fuzzball. The rigid rod is a straight rod of length L and cross sectional area A . The rigid rod is a WLC in the limit as $\ell_p \rightarrow \infty$. Because it has no flexibility, the rigid rod has no relevant internal energy E_{poly} . The fuzzball, like the rigid rod, has a single direction and no internal energy. However, the density of the fuzzball is spread out in a symmetric Gaussian about a point. The fuzzball can be thought of as a crude model of a small molecule or an electric quadrupole whose field falls off as a Gaussian.

III. SUMMARY OF DERIVATION

The results of this paper are intended to be intelligible without consulting the derivation. However, the derivation contains a number of interesting tricks and insights that the reader may find useful for similar problems. In particular, we describe a real spherical harmonic tensor distribution, extended summation notation for describing orientation over space, mean field polymer field theory, fluctuations away from this mean field, and WLC propagators derived via stone fence diagrams.

In this summary we provide a brief description of the approach we use to calculate the Frank elastic constants for a solution of semiflexible polymers. A similar procedure is followed for the rigid rod and fuzz-ball examples. We begin by describing the polymer solution with the partition function

$$Z \propto \int \mathcal{D}[\vec{r}_j(s)] \exp(-E_{poly} - E_{FH} - E_{MS}) \quad (3)$$

where the polymer bending energy E_{poly} is given in equation 2, the E_{FH} is the Flory-Huggins interaction and E_{MS} is the Maier-Saupe energy representing the preference for nearby polymers to align. The latter two are given by the sum of pairwise interactions

$$E_{FH} = \frac{A^2}{2} \sum_{i=1}^{n_p} \int_0^L ds_1 \sum_{j=1}^{n_p} \int_0^L ds_2 \chi \delta(\vec{r}_i(s_1) - \vec{r}_j(s_2)) \quad (4)$$

and

$$E_{MS} = \frac{A^2}{3} \sum_{i=1}^{n_p} \int_0^L ds_1 \sum_{j=1}^{n_p} \int_0^L ds_2 a(\vec{u}_i(s_1) \cdot \vec{u}_j(s_2))^2 \delta(\vec{r}_i(s_1) - \vec{r}_j(s_2)). \quad (5)$$

where A is the cross sectional area of the polymers. A factor of $1/2$ is included to account for double counting [24].

Equations 3-5 are then simplified significantly by using the local density and orientation distribution, ϕ , which we define in equation 7 and use throughout the remainder of the derivation. In this notation E_{FH} and E_{MS} are replaced with $\phi V \phi$ where V is the interaction matrix defined in equation 11.

To make the system mathematically tractable we first solve the partition function for the mean field of ϕ which we write as $\langle \phi \rangle^{MF}$. The self consistent equation 21 requires that $\langle \phi \rangle^{MF}$ is the density that would be expected in a field $\langle \phi \rangle^{MF} V$ which $\langle \phi \rangle^{MF}$ generates and applies to itself. The Frank elastic constants are defined in terms of fluctuations about this mean field solution, as will be discussed shortly.

In order to calculate ϕ for a WLC in the presence of an aligning mean field we follow [11, 21, 25] in using stone fence diagrams. These diagrams allow us to calculate the Laplace transform (from chain length N to Laplace variable p) of $\langle \phi \rangle$ as well as the Laplace transforms of products, e.g. $\mathcal{L}_{N \rightarrow p} \langle \phi_1 \phi_2 \rangle$. We are able to numerically invert the Laplace transforms via path integration in the complex plane. The construction of expectation values is described in section VIII and the description of the diagrams is given in section VII.

In section IX we investigate fluctuations about the mean field solution. The fluctuations are divided into Fourier modes via a Fourier transform from position \vec{r} to wave vector \vec{k} . To first approximation, the energy of each mode $\tilde{\phi}(\vec{k})$ is quadratic,

$$E \approx \tilde{\phi}(\vec{k}) \Gamma(\vec{k}) \tilde{\phi}(-\vec{k}) \quad (6)$$

where the “spring constants” for each of these modes are combined in the matrix Γ .

In section XIII we define the nematic director and the Frank elastic constants and manipulate them to be written in terms of particular long-wavelength elements of Γ . This allows us to write expressions for the Frank elastic constants in terms of numerical inverse Laplace transforms in section XV. The numerical evaluation of the inverse transform is described in section XVI.

IV. SUMMATION NOTATION & SYSTEM DESCRIPTION

The material properties at a point \vec{r} in space are determined by the position and orientation of polymers in the vicinity of \vec{r} . For a particular configuration $\{\vec{r}_j(s)\}$ of the system, the local density and orientation distributions can

be mathematically described by

$$\hat{\phi}_{\ell,m}(\vec{r}) \equiv \sqrt{\frac{4\pi}{2\ell+1}} \sum_{j=1}^{n_p} A \int_0^L ds Y_{\ell,m}(\vec{u}_j(s)) \delta(\vec{r} - \vec{r}_j(s)) \quad (7)$$

where $Y_{\ell,m}$ is the real spherical harmonic function described in appendix A. Note that we will use the roman \vec{r} and \vec{u} for position and orientation of points along a polymer and italicized \vec{r} and \vec{u} for generic position in space. These continuous polymers (assumption 2) could be replaced with discrete beads by replacing the integral in equation 7 with a sum. While $\hat{\phi}$ is formally defined as sum of infinitely thin space curve delta distributions, it is easier to interpret after integrating over a coarse grained volume ΔV in the vicinity of the position \vec{r} in the material. For example, the scalar component of the density $\hat{\phi}_{0,0}$ is interpreted as the local volume fraction of polymer; integrating $\hat{\phi}_{0,0}$ over the region of space ΔV gives the volume of polymer within that region. The values of $\hat{\phi}_{\ell,m}(\vec{r})$ for $\ell > 0$ describe the degree and direction of alignment of the polymers. In equation 7 the units of volume from $Ad s$ cancel the volume units from the delta function so that $\hat{\phi}$ is unitless, as would be expected from a volume fraction.

We write the partition function describing the set of configurations that $\hat{\phi}$ can take on as

$$Z = \frac{1}{n_p!} \int \mathcal{D}[\vec{r}_j(s)] \exp\left(-E_{poly} - \frac{1}{2} \hat{\phi}_1 V_{12} \hat{\phi}_2\right) \quad (8)$$

The $1/n_p!$ prefactor accounts for the indistinguishability of the polymers but is not consequential the following discussion. The functional integral $\int \mathcal{D}[\vec{r}_j(s)]$ refers to an integral over all possible configurations of the system, that is, it integrates the position of each point of each polymer over all space

$$\int \mathcal{D}[\vec{r}_j(s)] = \lim_{\Delta s \rightarrow 0} \prod_{j=1}^{n_p} \int_{-\infty}^{\infty} d\vec{r}_{j,s=0} \int_{-\infty}^{\infty} d\vec{r}_{j,s+\Delta s} \dots \int_{-\infty}^{\infty} d\vec{r}_{j,L} \quad (9)$$

The WLC polymer energy E_{poly} defined in equation 2 effectively reduces the region of integration to continuous smooth polymers. The term $\frac{1}{2} \hat{\phi}_1 V_{12} \hat{\phi}_2$ in equation 8 describes the interaction potential between polymers. The interaction is quadratic in $\hat{\phi}$ in keeping with assumption 9. The subscripts in $\hat{\phi}_1 V_{12} \hat{\phi}_2$ refer to an extended summation notation that sums over ℓ and m indices and integrates over space such that

$$\hat{\phi}_1 V_{12} \hat{\phi}_2 \equiv \sum_{\ell_1=0}^{\infty} \sum_{m_1=-\ell_1}^{\ell_1} \sum_{\ell_2=0}^{\infty} \sum_{m_2=-\ell_2}^{\ell_2} \int d\vec{r}_1 d\vec{r}_2 \hat{\phi}_{\ell_1,m_1}(\vec{r}_1) V_{\ell_1,\ell_2}^{m_1,m_2}(\vec{r}_1, \vec{r}_2) \hat{\phi}_{\ell_2,m_2}(\vec{r}_2) \quad (10)$$

Combining the concise summation notation with the spherical harmonic indices for orientation allows us to manipulate the tensor field $\hat{\phi}$ in much the same way as scalar fields in previous publications [26, 27]. Note that when ϕ has a single subscript this is understood to be the subscript from the summation notation and when it has two as in $\phi_{\ell,m}$ these refer to ℓ and m as should also be clear from context. The notation $\hat{\phi}_1 V_{12} \hat{\phi}_2$ is analogous to the vector notation $\vec{\phi}^T V \vec{\phi}$ for matrix V and vector $\vec{\phi}$ which have an infinite number of indices in order to capture all ℓ, m , and \vec{r} . While this notation allows for a wide variety of orientationally dependent and ranged potentials, we will restrict our discussion to local potentials (assumption 10) with $V \propto \delta(\vec{r}_1 - \vec{r}_2)$. We will also restrict V to be non-zero only for a Flory-Huggins scalar potential ($\ell = 0$) and a Maier-Saupe tensor potential ($\ell = 2$) in keeping with assumption 11. Interactions of order $\ell = 1$ violate the assumed reversal symmetry (assumption 6). Including interaction terms of order $\ell > 2$ would relax assumption 11 to systematically refine the rotational detail of inter-chain interactions with the interaction constants depending on the chemistry and sterics of the polymer in question.

Under the above assumptions we write

$$V_{12} = \left(\chi \delta_{\ell_1,0} - \frac{2}{3} a \delta_{\ell_1,2} \right) \delta_{m_1,m_2} \delta_{\ell_1,\ell_2} \delta(\vec{r}_1 - \vec{r}_2) \quad (11)$$

where χ is the widely used Flory-Huggins mixing parameter. The second term in the parentheses provides an energetic benefit to polymer segments that align $\vec{u}_1 \approx \vec{u}_2$ or antialign $\vec{u}_1 \approx -\vec{u}_2$. The factor of $2/3$ maintains the meaning of the Maier-Saupe parameter, a , from [10] and [11]. The negative sign on the $\ell = 2$ term in equation 11 is chosen so that a positive a corresponds to a preferential alignment. The equivalence to the Maier-Saupe formulation [10, 11] in terms of $\vec{u} \otimes \vec{u} - \frac{1}{3} I$ rather than $Y_2^m(\vec{u})$ results from the relation

$$\sum_{i,j=1}^3 \left(\vec{u}_1 \otimes \vec{u}_1 - \frac{1}{3} I \right)_{ij} \left(\vec{u}_2 \otimes \vec{u}_2 - \frac{1}{3} I \right)_{ij} = (\vec{u}_1 \cdot \vec{u}_2)^2 - \frac{1}{3} = \frac{2}{3} P_2(\vec{u}_1 \cdot \vec{u}_2) = \frac{2}{3} \sum_{m=-2}^2 Y_{2,m}(\vec{u}_1) Y_{2,m}(\vec{u}_2) \quad (12)$$

for all unit vectors \vec{u}_1 and \vec{u}_2 .

Fuzzball and Rigid Rod

In contrast to equation 7, the density distribution for solution of fuzzballs is given as

$$\hat{\phi}_{\ell,m}^{FB} = \sqrt{\frac{4\pi}{2\ell+1}} \sum_{j=1}^{n_p} \frac{v_p}{(2\pi\sigma^2)^{3/2}} \exp\left(-\frac{(\vec{r}-\vec{r}_j)^2}{2\sigma^2}\right) Y_{\ell,m}(\vec{u}_j) \quad (13)$$

where σ is the standard deviation of the field falloff and defines the size of the fuzzball. v_p is the effective volume (or amplitude if you prefer) of the fuzzball. For rigid rods the density distribution is

$$\hat{\phi}_{\ell,m}^{RR}(\vec{r}) = \sqrt{\frac{4\pi}{2\ell+1}} \sum_{j=1}^{n_p} Y_{\ell,m}(\vec{u}_j) A \int_0^L ds \delta(\vec{r}_j + s\vec{u}_j - \vec{r}) \quad (14)$$

where \vec{r}_j is the location of one end of the rod and \vec{u}_j is the orientation of the rod. For the rigid rod, the integration in the above equation simplifies to

$$\hat{\phi}_{\ell,m}^{RR}(\vec{r}) = \sqrt{\frac{4\pi}{2\ell+1}} \sum_{j=1}^{n_p} Y_{\ell,m}(\vec{u}_j) AL \delta(\vec{r}_j + L\vec{u}_j - \vec{r})$$

The partition functions for these two solutions are similar

$$Z^{RR/FB} = \int d\vec{r}_j \int d\vec{u}_j \exp\left(\frac{1}{2}\chi\left(\phi_{0,0}^{RR/FB}(\vec{r})\right)^2 + \frac{1}{3}a \int d\vec{r} \sum_{m=-2}^2 \left(\phi_{2,m}^{RR/FB}(\vec{r})\right)^2\right) \quad (15)$$

and, in contrast to the WLC, simply require integrating over n_p positions \vec{r}_j and n_p orientations \vec{u}_j .

V. FIELD MANIPULATIONS

We introduce a delta function at every point in space and orientation $\delta(\phi - \hat{\phi})$. Extending the Fourier representation of a delta function $\delta(a-b) = \frac{1}{2\pi} \int_{-\infty}^{\infty} dp (ip(a-b))$ to a delta function for a tensor distribution ϕ we have

$$\delta(\phi - \hat{\phi}) \propto \int \mathcal{D}W \exp\left(iW_1(\phi_1 - \hat{\phi}_1)\right) \quad (16)$$

where the functional integral $\int \mathcal{D}W$ integrates $W_\ell^m(\vec{r})$ for each \vec{r} , ℓ , and m combination. Like ϕ , the Fourier variable W is also a tensor distribution. Inserting this delta function into the partition function (equation 8) in the fashion of $f(x) = \int dy f(y) \delta(x-y)$ we have

$$Z \propto \int \mathcal{D}W \mathcal{D}\phi \mathcal{D}\left[\vec{r}^{(1)}(s)\right] e^{-E_{poly} - \frac{1}{2}\phi_1 V_{12}\phi_2 + iW_1(\phi_1 - \hat{\phi}_1)} \quad (17)$$

Note that the E_{poly} and $\hat{\phi}$ only depend on \vec{r} while $\phi_1 V_{12}\phi_2$ and $W_1\phi_1$ only depend on ϕ so these terms can be separated

$$Z \propto \int \mathcal{D}W \mathcal{D}\phi e^{-\frac{1}{2}\phi_1 V_{12}\phi_2 + iW_1\phi_1} \left[\int \mathcal{D}\vec{r}^{(1)} e^{-E_{poly}^{(1)} - iW_1\hat{\phi}_1^{(1)}} \right]^{n_p} \quad (18)$$

This separation is quite useful, and is why we introduced the delta function 16 and the W field.

The second integral in 18 contains no inter-chain interactions other than through the W field and all chains are identical (assumption 1) so it has been factored into a product of n_p terms. The superscript ⁽¹⁾ on \vec{r} , E_{poly} , and $\hat{\phi}$ indicates a single chain. Defining the contents of the square bracket in equation 18 as z_p we have

$$Z \propto \int \mathcal{D}W \mathcal{D}\phi e^{-\frac{1}{2}\phi_1 V_{12}\phi_2 + iW_1\phi_1 + n_p \ln(z_p)} \quad (19)$$

$$z_p = \int \mathcal{D} [\vec{r}^{(1)}(s)] e^{-E_{poly}^{(1)} - iW_1 \hat{\phi}_1^{(1)}} \quad (20)$$

While strictly speaking W is simply an integration variable, we can assign a physical meaning to it as a chemical potential. The term iW_1 in equation 20 is the effective potential experienced by a single polymer. Meanwhile, the term iW_1 in equation 19 represents the potential that the single polymers impose to deform the density field ϕ . In this way single polymers don't communicate directly with each other, but communicate through the local chemical potential W . We will later integrate out W between equations 64 and 66.

VI. MEAN FIELD SOLUTION

A. Mean Field Solution for Polymer Solutions

In this section we will solve for the homogeneous mean field solution $\hat{\phi}$ of partition function 8 so that we can expand about $\hat{\phi}$ in section IX. The essence of the mean field solution is that rather than calculating all interactions inside and between polymers, we calculate the statistics of a single polymer with E_{FH} and E_{MS} replaced by the average field the polymer experiences. The self consistency requirement sets the mean field strength to that generated by n_p such single polymers. The field experienced by a single polymer can be found by differentiating the potential $\frac{1}{2}\hat{\phi}_1 V_{12} \hat{\phi}_2$ with respect to the field generated by a single polymer, $\hat{\phi}^{(1)}$, to get $\langle \phi \rangle_1^{MF} V_{12}$. The self consistent equation sets the expectation value of $n_p \langle \hat{\phi}^{(1)} \rangle$ to be the mean field strength $\langle \phi \rangle^{MF}$.

$$\langle \phi \rangle^{MF} = \frac{\int \mathcal{D} [\vec{r}^{(1)}] n_p \hat{\phi}^{(1)} \exp \left(-E_{poly} - \langle \phi \rangle_1^{MF} V_{12} \hat{\phi}_2^{(1)} \right)}{\int \mathcal{D} [\vec{r}^{(1)}] \exp \left(-E_{poly} - \langle \phi \rangle_1^{MF} V_{12} \hat{\phi}_2^{(1)} \right)} \quad (21)$$

Equation 21 can alternatively be derived by introducing W as was done in equations 19 and 20 and then minimizing the integrand of equation 19 with respect to a constant ϕ and W which gives $\langle \phi \rangle^{MF}$ and $iW_1^{MF} = V_{12} \langle \phi \rangle_2^{MF}$.

For values of the Maier-Saupe parameter a below its critical value a^* , the homogeneous mean field solution will simply be a constant density with no net alignment $\langle \phi \rangle_{\ell,m}^{MF} = \langle \phi \rangle_{0,0}^{MF} \delta_{\ell,0}$. Above a^* the tendency for polymers to align will overpower entropy and break rotational symmetry creating a direction of preferred orientation. We will align this direction with the \hat{z} axis. Because the mean field solution is constant throughout all space (assumptions 7 and 8) the $\ell = 0$ component of $\langle \phi \rangle_{\ell,m}^{MF} = \langle \phi \rangle_{0,0}^{MF} \delta_{\ell,0} + \langle \phi \rangle_{2,0}^{MF} \delta_{\ell,0} \delta_{m,0}$. Because $\langle \phi \rangle_{0,0}^{MF}$ is a constant scalar offset it can be canceled from equation 21 with no consequence. However, there will be a non-zero $\phi_{2,0}$ which will need to be solved for. Under the potential 11, the aligning field energy for a single polymer is $\langle \phi \rangle_1^{MF} V_{12} \hat{\phi}_2^{(1)} = -\gamma \int_0^N ds Y_{2,0}(\vec{u}(s))$ where $N = L/2\ell_p$ is chain length nondimensionalized by the Kuhn length[28] and

$$\gamma = \frac{2}{3} \sqrt{\frac{4\pi}{5}} 2\ell_p A a \langle \phi \rangle_{2,0}^{MF} \quad (22)$$

is the strength of the aligning field which follows from equations 11 and 7. The value of gamma can roughly be thought of as the aligning energy in kT 's per persistence length of polymer.

The procedure for calculating the value of $\langle \phi \rangle_{2,0}^{MF}$ as a function of γ will be derived below, resulting in formula 59 with the inverse Laplace transform being performed numerically as described in section XVI. In figure 2 we plot the mean field strength γ in terms of a . These are plotted by solving 22 for a as a function of γ .

$$a = \frac{\gamma}{\frac{2}{3} \sqrt{\frac{4\pi}{5}} 2\ell_p A \langle \phi \rangle_{2,0}^{MF}(\gamma)} \quad (23)$$

When working with relatively stiff polymers $L < 2\ell_p$ it is natural to nondimensionalize a by the polymer volume LA . When working with flexible polymers it is natural to nondimensionalize a by the volume of a Kuhn length $2\ell_p A$. Because a stronger a is needed in dilute solutions, it is also convenient to multiply a by the volume fraction of polymer $\phi_{0,0}$.

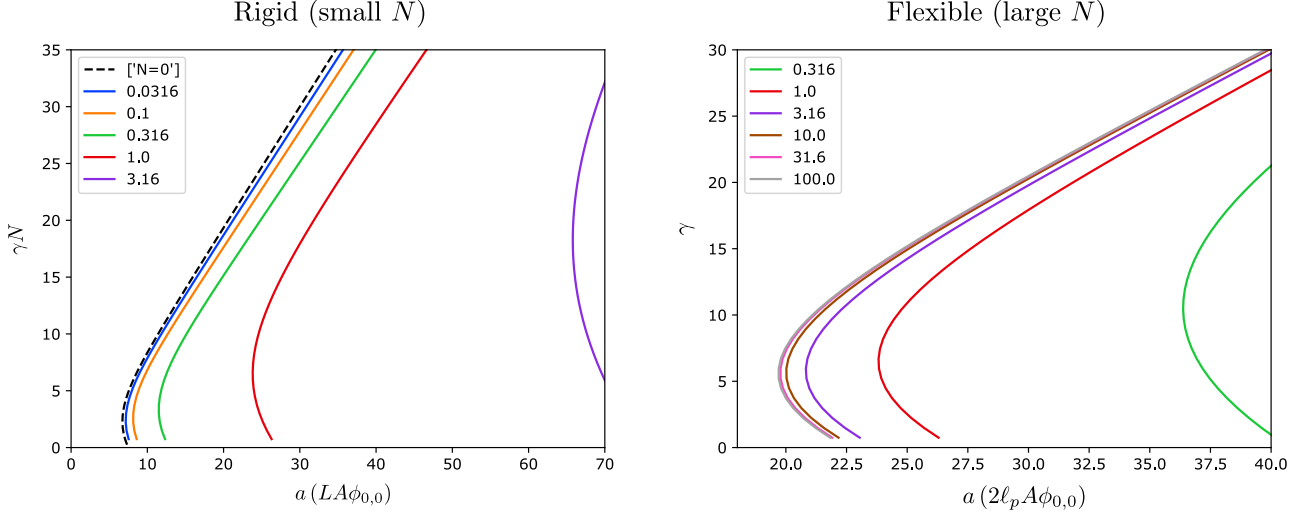


FIG. 2. Mean field strength γ as a function of Maier-Saupe a . The lower branch is nonphysical; the nose corresponds to the limit of meta-stability of the aligned phase. Curves are colored by the length of the polymer in Kuhn lengths, N . The left plot is nondimensionalized by polymer length, which is convenient for rigid polymers. The right plot is nondimensionalized by $2\ell_p$, which is convenient for flexible polymers. The dashed curve represents the rigid rod.

B. Mean Field Solution for Rigid Rod and Fuzzball

As the fuzzball and rigid rod have no Kuhn length, we instead define their field strengths γ in terms of their respective volumes

$$\gamma^{FB} = \frac{2}{3} a \langle \phi_{2,0} \rangle^{MF} \sqrt{\frac{4\pi}{5}} v_p \quad (24)$$

$$\gamma^{RR} = \frac{2}{3} a \langle \phi_{2,0} \rangle^{MF} \sqrt{\frac{4\pi}{5}} LA \quad (25)$$

so that the energy associated with each object is $E^{(1)} = -\gamma Y_{2,0}(\vec{u}_i)$. The partition function for the orientation of a single fuzzball or rigid rod is given by

$$z^{FB/RR} = \int d\vec{u}_i \exp(\gamma Y_{2,0}(\vec{u}_i)) \quad (26)$$

To calculate expectation values for this partition function it is useful to define the matrix

$$\mathbf{M}_{\ell_1, \ell_2}^m = \int d\vec{u}_i Y_{\ell_1, m}(\vec{u}_i) \exp(\gamma Y_{2,0}(\vec{u}_i)) Y_{\ell_2, m}(\vec{u}_i) \quad (27)$$

The numerical values of \mathbf{M} can be obtained by matrix exponentiation

$$\mathbf{M}^m = \exp\left(\gamma \mathbf{J}_{(2)}^{m,0,m}\right) \quad (28)$$

where

$$\left(\mathbf{J}_{(2)}^{m,0,m}\right)_{\ell_1, \ell_2} = \int d\vec{u} Y_{\ell_1, m}(\vec{u}) Y_{2,0}(\vec{u}) Y_{\ell_2, m}(\vec{u}) \quad (29)$$

which is given in appendix A. As an example of how \mathbf{M} can be used to calculate an expectation, consider

$$\left\langle \phi_{\ell, m}^{RR/FB} \right\rangle^{MF} = n_p \frac{\int d\vec{r} \int d\vec{u} \exp(\gamma Y_{2,0}(\vec{u}_j)) \phi_{\ell, m}^{(1)RR/FB}}{\int d\vec{r} \int d\vec{u} \exp(\gamma Y_{2,0}(\vec{u}_j))} \quad (30)$$

which, with the help of $Y_{0,0} = \frac{1}{\sqrt{4\pi}}$, simplifies to

$$\langle \phi_{\ell,m}^{RR} \rangle^{MF} = \frac{n_p AL}{\mathcal{V}} \sqrt{\frac{1}{2\ell+1}} \frac{\mathbf{M}_{0,\ell_2}^0}{\mathbf{M}_{0,0}^0} \delta_{m,0} \quad (31)$$

$$\langle \phi_{\ell,m}^{FB} \rangle^{MF} = \frac{n_p v_p}{\mathcal{V}} \frac{1}{\sqrt{2\ell+1}} \frac{\mathbf{M}_{0,\ell}^0}{\mathbf{M}_{0,0}^0} \delta_{m,0}. \quad (32)$$

From the above we can verify the densities, $\langle \phi_{0,0}^{RR} \rangle^{MF} = \frac{n_p AL}{\mathcal{V}}$ and $\langle \phi_{0,0}^{FB} \rangle^{MF} = \frac{n_p v_p}{\mathcal{V}}$, and get the mean field alignment $\langle \phi_{0,2}^{RR/FB} \rangle^{MF}$ and then solve for the Maier-Saupe parameter

$$a^{RR} LA\phi_{00} = \frac{15\gamma^{RR} \mathbf{M}_{0,0}^0 (\gamma^{RR})}{4\sqrt{\pi} \mathbf{M}_{0,2}^0 (\gamma^{RR})} \quad (33)$$

$$a^{FB} v_p \phi_{00} = \frac{15\gamma^{FB} \mathbf{M}_{0,0}^0 (\gamma^{FB})}{4\sqrt{\pi} \mathbf{M}_{0,2}^0 (\gamma^{FB})} \quad (34)$$

plotted in figure 2.

VII. STONE FENCE DIAGRAMS

In this section we derive a propagator – equations 51 and 52 – which we will use to calculate $\langle \phi \rangle^{MF}$ in the next section.

To obtain a numerical value of $\langle \phi \rangle^{MF}$ we follow the approach of [11, 21, 22] beginning with the propagator for a semi-flexible WLC (assumption 3) without an aligning field [21] (i.e. as if $\langle \phi \rangle_2^{MF} = 0$):

$$G_o(\vec{u}|\vec{u}_0; L) = \sum_{\ell=0}^{\infty} \sum_{m=-\ell}^{\ell} Y_{\ell,m}(\vec{u}) Y_{\ell,m}(\vec{u}_0) e^{-\ell(\ell+1)\frac{L}{2\ell_p}} \quad (35)$$

which gives the probability distribution for the orientation \vec{u} at one end of a chain of length L , given that the other end is orientated in the \vec{u}_0 direction. (Note that in [21] complex spherical harmonics were used. Because $\sum_{m=-\ell}^{\ell} Y_{\ell}^m(\vec{u}) Y_{\ell}^{m*}(\vec{u}_0) = P_{\ell}(\vec{u} \cdot \vec{u}_0) = \sum_{m=-\ell}^{\ell} Y_{\ell,m}(\vec{u}) Y_{\ell,m}(\vec{u}_0)$ equation 35 also holds for real spherical harmonics.) G_o ranges between the rigid rod $\lim_{L/2\ell_p \rightarrow 0} G_o(\vec{u}|\vec{u}_0; L) = \delta(\vec{u} - \vec{u}_0)$ and flexible chain $\lim_{L/2\ell_p \rightarrow \infty} G_o(\vec{u}|\vec{u}_0; L) = \frac{1}{4\pi}$ and has the property $G_o(\vec{u}|\vec{u}_0; L) = \int d\vec{u}_1 G_o(\vec{u}_1|\vec{u}_0; L_1) G_o(\vec{u}|\vec{u}_1; L - L_1)$ where $\int d\vec{u}_1$ is meant as integration over the unit sphere. Going forward we will nondimensionalize the polymer length by the Kuhn length $2\ell_p$ to give $N = L/2\ell_p$.

The propagator G_o allows us to calculate statistics about any point along a free chain. For example, suppose we have a WLC constrained to start from orientation \vec{u}_0 and end at orientation \vec{u}_f and there is some function f that depends on the orientation \vec{u}_1 at a point $N_1 = L_1/2\ell_p$ along a polymer. We can calculate f 's expectation value via

$$\langle f(\vec{u}_1) \rangle_o = \frac{\int d\vec{u}_1 G_o(\vec{u}_1|\vec{u}_0; N_1) f(\vec{u}_1) G_o(\vec{u}_f|\vec{u}_1; N - N_1)}{G_o(\vec{u}_f|\vec{u}_0; N)} \quad (36)$$

This expectation value is precisely the type of quantity that we need to calculate to obtain the propagator G for a WLC which is in an aligning field $\phi_1^{MF} V_{12}$ from equation 21. In particular, if we use the expectation value in equation 36 to include the aligning field γ as a re-weighting of G_o then the partition function for the end orientation is

$$G(\vec{u}_f|\vec{u}_0; N) = G_o(\vec{u}_f|\vec{u}_0; N) \left\langle \exp \left[\gamma \int_0^N ds Y_{2,0}(\vec{u}(s)) \right] \right\rangle_o \quad (37)$$

where the prefactor $G_o(\vec{u}_f|\vec{u}_0; N)$ cancels the denominator of 36. Please note that G is an unnormalized distribution that is proportional to the probability distribution of \vec{u}_f for a given \vec{u}_0 ,

$$P(\vec{u}_f|\vec{u}_0; N) = \frac{G(\vec{u}_f, \vec{u}_0, N)}{\int d\vec{u}'_f G(\vec{u}'_f, \vec{u}_0, N)}. \quad (38)$$

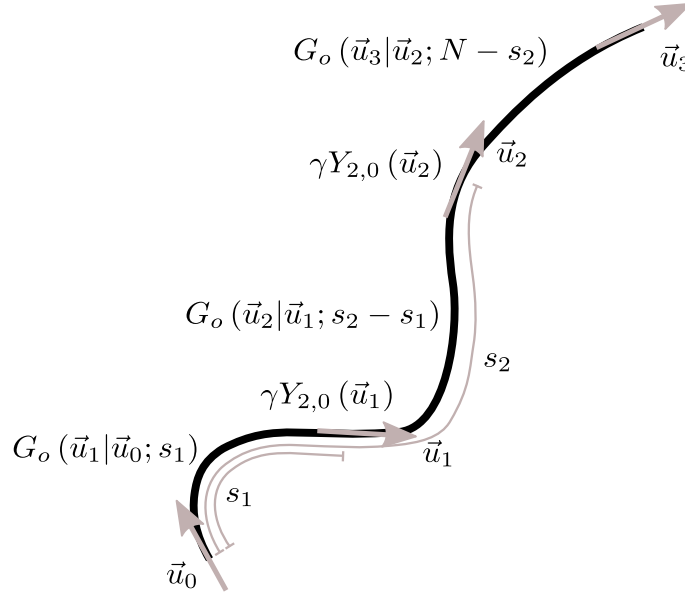


FIG. 3. Schematic illustrating the right hand side of equation 42. The thick black curve represents a polymer N Kuhn lengths long. Arrows represent unit vectors $\vec{u}_0, \vec{u}_1, \vec{u}_2, \vec{u}_3$ at path lengths 0, s_1 , s_2 , and N along the polymer respectively.

P and G differ in that $\frac{1}{4\pi} \int d\vec{u}_0 P(\vec{u}_f|\vec{u}_0; N)$ gives the probability distribution of \vec{u}_f assuming \vec{u}_0 is uniform over the unit sphere, while $\frac{1}{4\pi} \int d\vec{u}_0 G(\vec{u}_f|\vec{u}_0; N)$ is proportional to the probability distribution of \vec{u}_f for a polymer of length N in an aligning field whose ends are free to rotate. Like G_0 , the propagator G has the property $G(\vec{u}|\vec{u}_0; L) = \int d\vec{u}_1 G(\vec{u}_1|\vec{u}_0; L_1) G(\vec{u}|\vec{u}_1; L - L_1)$. We can think of $G(\vec{u}|\vec{u}_0; L)$ as the partition function for \vec{u} and \vec{u}_0 . The quantity $G(\vec{u}|\vec{u}_0; L)$ is useful because it allows us to calculate chain statistics in the presence of the γ field. For example, the expectation of $f(\vec{u}_1)$ for a chain in field of strength γ and freely rotating ends is given by

$$\langle f(\vec{u}_1) \rangle = \frac{\int d\vec{u}_0 \int d\vec{u}_1 \int d\vec{u}_f G(\vec{u}_1|\vec{u}_0; L_1) f(\vec{u}_1) G(\vec{u}_f|\vec{u}_1; L - L_1)}{\int d\vec{u}_0 \int d\vec{u}_1 \int d\vec{u}_f G(\vec{u}_1|\vec{u}_0; L_1) G(\vec{u}_f|\vec{u}_1; L - L_1)} \quad (39)$$

where the denominator can be simplified to $\int d\vec{u}_0 \int d\vec{u}_f G(\vec{u}_f|\vec{u}_0; L)$.

We now turn to calculating $G(\vec{u}|\vec{u}_0; L)$. Whereas equation 36 depended only on the orientation at s_1 , the expectation value in equation 37 depends on the orientation at every point along the chain. In order to expand G in terms of G_o , we Taylor expand the exponential and reorder the integrals

$$\exp \left[\gamma \int_0^N ds Y_{2,0}(\vec{u}(s)) \right] = \sum_{n=0}^{\infty} \frac{1}{n!} \left(\gamma \int_0^N ds Y_{2,0}(\vec{u}(s)) \right)^n \quad (40)$$

$$= \sum_{n=0}^{\infty} \left(\gamma^n \int_0^N ds_n \dots \int_0^{s_3} ds_2 \int_0^{s_2} ds_1 \prod_i^n Y_{2,0}(\vec{u}_i) \right) \quad (41)$$

where we have introduced the short hand $\vec{u}_i \equiv \vec{u}(s_i)$. The factor of $\frac{1}{n!}$ canceled the $n!$ from ordering the integrals. To calculate the the $n = 2$ term, for example, we have

$$\begin{aligned} & \left\langle \gamma^2 \int_0^N ds_2 \int_0^{s_2} ds_1 Y_{2,0}(\vec{u}_2) Y_{2,0}(\vec{u}_1) \right\rangle_o \\ &= \gamma^2 \int_0^N ds_2 \int_0^{s_2} ds_1 \int d\vec{u}_2 \int d\vec{u}_1 G_o(\vec{u}_3|\vec{u}_2; N - s_2) Y_{2,0}(\vec{u}_2) G_o(\vec{u}_2|\vec{u}_1; s_2 - s_1) Y_{2,0}(\vec{u}_1) G_o(\vec{u}_1|\vec{u}_0; s_1) \end{aligned} \quad (42)$$

To simplify equation 42, it is convenient to perform a Laplace transform from $N \rightarrow p$. Defining the Laplace transform of equation 35 as $\check{G}_o(p) \equiv \mathcal{L}[G] = \int_0^\infty dN G_o(N) e^{-pN}$ gives

$$\check{G}_o(\vec{u}|\vec{u}_0; p) = \sum_{\ell=0}^{\infty} \sum_{m=-\ell}^{\ell} Y_{\ell,m}(\vec{u}_f) Y_{\ell,m}(\vec{u}_0) \frac{1}{p + \ell(\ell + 1)} \quad (43)$$

The convolution rule for Laplace transforms says that $\mathcal{L}(f)\mathcal{L}(g) = \mathcal{L}[f * g] = \mathcal{L}\left[\int_0^t d\tau f(\tau)g(t-\tau)\right]$. In equation 42 we have something of the form $\mathcal{L}[f * g * h]$. By plugging the convolution rule into itself recursively we arrive at the general relation $\mathcal{L}[f_1 * f_2 * \dots f_{n+1}] = \prod_{j=1}^{n+1} \mathcal{L}(f_j)$. Taking the Laplace transform of the $n = 2$ example in equation 42 and substituting into 43 we arrive at

$$\begin{aligned} \mathcal{L}[\langle \dots \rangle_o] &= \sum_{\ell_i, m_i} Y_{\ell_1, m_1}(\vec{u}_0) \\ &\times \check{G}_o(p|\ell_1) \gamma \int d\vec{u}_1 Y_{\ell_1, m_1}(\vec{u}_1) Y_{2,0}(\vec{u}_1) Y_{\ell_2, m_2}(\vec{u}_1) \\ &\times \check{G}_o(p|\ell_2) \gamma \int d\vec{u}_2 Y_{\ell_2, m_2}(\vec{u}_2) Y_{2,0}(\vec{u}_2) Y_{\ell_3, m_3}(\vec{u}_2) \\ &\times \check{G}_o(p|\ell_3) Y_{\ell_3, m_3}(\vec{u}_f) \end{aligned} \quad (44)$$

where $\langle \dots \rangle_o = \left\langle \gamma^2 \int_0^N ds_2 \int_0^{s_2} s_1 Y_{2,0}(\vec{u}_2) Y_{2,0}(\vec{u}_1) \right\rangle_o$ and $\check{G}_o(p|\ell) \equiv \frac{1}{p+\ell(\ell+1)}$ from equation 43. The integrals over the spherical harmonics in the middle can be written in terms of A_ℓ^m and β_ℓ^m from appendix A. In particular equation A11 gives us

$$\int d\vec{u}_1 Y_{\ell_1, m_1}(\vec{u}_1) Y_{2,0}(\vec{u}_1) Y_{\ell_2, m_2}(\vec{u}_1) = (A_{\ell_1+2}^{m_1} \delta_{\ell_1+2, \ell_2} + \beta_{\ell_1}^{m_1} \delta_{\ell_1, \ell_2} + A_{\ell_1}^{m_1} \delta_{\ell_1-2, \ell_2}) \delta_{m_1, m_2} \quad (45)$$

so that

$$\begin{aligned} \mathcal{L}[\langle \dots \rangle_o] &= \sum_{\ell_1, m} Y_{\ell_1, m}(\vec{u}_0) \check{G}_o(p|\ell_1) \\ &\times (A_{\ell_1+2}^m \delta_{\ell_1+2, \ell_2} + \beta_{\ell_1}^m \delta_{\ell_1, \ell_2} + A_{\ell_1}^m \delta_{\ell_1-2, \ell_2}) \\ &\times \check{G}_o(p|\ell_2) \\ &\times (A_{\ell_2+2}^m \delta_{\ell_2+2, \ell_3} + \beta_{\ell_2}^m \delta_{\ell_2, \ell_3} + A_{\ell_2}^m \delta_{\ell_2-2, \ell_3}) \\ &\times \check{G}_o(p|\ell_3) Y_{\ell_3, m}(\vec{u}_f) \end{aligned} \quad (46)$$

which distributes to 9 terms for each m and ℓ_1 (though some are disallowed by the requirements that $\ell_1 \geq |m|$).

We would like to apply the reasoning of equations 44 and 45 to all term in the sum 40, the Laplace transform of $G(\vec{u}_f, \vec{u}_0, N)$. However, multiplying 45 by itself for each of the terms in 40 will result in a very large number of terms. The enumeration of these terms is greatly aided by the use of stone fence diagrams [21, 22, 25]. Each diagram represents a term, with the sum of all diagrams equaling $G(\vec{u}_f, \vec{u}_0, N)$. The simplest such diagram – and only type at the $n = 0$ level of 40 – is the orientation propagator without an aligning field $\langle \rangle_o = \check{G}_o(p|\ell_3)$ and represented by a dot:

$$\frac{1}{P_\ell} \equiv \frac{1}{p + \ell(\ell + 1)} \equiv \quad \ell \bullet$$

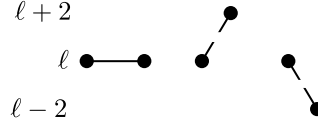
There is one of these diagrams for each of the values of ℓ – indicated by the ℓ to the left of the diagram. In this case, the incoming ℓ_0 and outgoing ℓ_f are always the same, as indicated by the same ℓ for the spherical harmonics of \vec{u}_f and \vec{u}_0 in equation 43. However, diagrams for $n > 0$, which include factors of γ , may connect different ℓ values. The form of equation 44 suggests that we should connect these dots with products of spherical harmonics. There are three types of connections in equation 45 corresponding to keeping the ℓ value the same, increasing ℓ by 2, or decreasing ℓ by 2. These are represented by horizontal, upwardly slanted, and downwardly slanted connections respectively:

$$\gamma \beta_\ell^m \equiv \quad \ell \text{ — } \ell$$

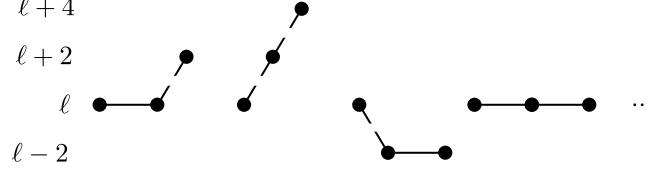
and

$$\gamma A_{\ell+2}^m \equiv \quad \begin{array}{c} \ell+2 \\ \diagup \\ \ell \end{array} = \quad \diagdown$$

in this way the vertical axis corresponds to ℓ as is indicated by the expressions to the left of the diagrams. The three possible diagrams starting at ℓ and having a single γ are



and 4 of the 9 possible diagrams proportional to γ^2 are



These nine diagrams correspond to the nine terms in equation 46. For each eigenvalue set $\{m_0, \ell_0\}$ describing the orientation of \vec{u}_0 , there are 3^n such diagrams from the γ^n term of the expansion 40; though many of these will be zero due to the requirement that $\ell \geq |m|$ which is enforced by $A_\ell^\ell = A_\ell^{\ell+1} = 0$ and disallows diagrams that go below $|m|$ anywhere along their path. Our task is to sum the allowed diagrams with any number, n , of sections. We define a new symbol to denote the sum of all such diagrams that don't contain any factors of A so that it starts and ends at ℓ .

$$\ell \quad \bullet \text{---} \bullet \quad \equiv \quad \bullet \text{---} \bullet \quad + \quad \bullet \text{---} \bullet \text{---} \bullet \quad + \quad \bullet \text{---} \bullet \text{---} \bullet \text{---} \bullet \quad + \quad \dots$$

which can be evaluated via a geometric series

$$\sum_{n=0}^{\infty} \left(\frac{1}{P_{\ell}} \right)^{n+1} (\gamma \beta_{\ell}^m)^n = \frac{1}{P_{\ell} - \gamma \beta_{\ell}^m} \quad (47)$$

The critical insight made in [21] is to sum all of the diagrams that start and end at ℓ but never stray below ℓ in between. We define this new quantity as

[illegible]

which can be summed with a geometric series

$$W_{\ell}^{(+m)} = \sum_{n=0}^{\infty} \left(\frac{1}{P_{\ell} - \gamma \beta_{\ell}^m} \right)^{n+1} \left((\gamma A_{\ell+2}^m)^2 W_{\ell+2}^{(+m)} \right)^n = \frac{1}{P_{\ell} - \gamma \beta_{\ell}^m - (\gamma A_{\ell+2}^m)^2 W_{\ell+2}^{(+m)}} \quad (48)$$

which can be calculated recursively by truncating at a sufficiently high ℓ value.

Likewise

$$W_\ell^{(-)m} \equiv \ell \quad \text{[diagram: a wavy line with two vertices and a downward arrow]} \\ \equiv \ell \quad \text{[diagram: a sequence of terms involving dashed lines, vertices, and wavy lines with downward arrows, including a label } \ell-2 \text{]} \dots$$

$$W_\ell^{(-)m} = \begin{cases} \frac{1}{P_\ell - \gamma B_\ell^m - (\gamma A_\ell^m)^2 W_{\ell-2}^{(-)m}} & \ell \geq |m| \\ 0 & \text{otherwise} \end{cases} \quad (49)$$

where we have explicitly cut off the recursion when ℓ dips below $|m|$.

Also of interest is the diagram similar to $W^{(+)}$ but without the left dot and requiring at least one up-down step

$$\begin{aligned}
(P_\ell - \gamma\beta_\ell^m) W_\ell^{(+m)} - 1 &\equiv \text{diagram: a circle with a dot on the right} \\
&\equiv \text{diagram: a wavy line starting at } \ell, \text{ with an up arrow, ending at } \ell+2, \text{ followed by a dashed line} \\
&\quad + \text{diagram: a wavy line starting at } \ell, \text{ with an up arrow, ending at } \ell+2, \text{ followed by a dashed line} \\
&\quad + \text{diagram: a wavy line starting at } \ell, \text{ with an up arrow, ending at } \ell+2, \text{ followed by a dashed line} \\
&\quad + \dots \\
(P_\ell - \gamma\beta_\ell^m) W_\ell^{(-m)} - 1 &\equiv \text{diagram: a circle with a dot on the left} \\
&\equiv \text{diagram: a wavy line starting at } \ell, \text{ with a down arrow, ending at } \ell-2, \text{ followed by a dashed line} \\
&\quad + \text{diagram: a wavy line starting at } \ell, \text{ with a down arrow, ending at } \ell-2, \text{ followed by a dashed line} \\
&\quad + \text{diagram: a wavy line starting at } \ell, \text{ with a down arrow, ending at } \ell-2, \text{ followed by a dashed line} \\
&\quad + \dots
\end{aligned}$$

To get all the diagrams that begin and end at ℓ we need to include all possible sets of up steps and down steps. We group these diagrams into four groups: 1, up first down last; 2, up first up last; 3, down first up last; and 4, down first down last.

$$\begin{aligned}
W_\ell^{(\pm)m} &\equiv \text{diagram: a wavy line starting at } \ell, \text{ with a double arrow, ending at } \ell \\
&\equiv \text{diagram: a wavy line starting at } \ell, \text{ with an up arrow, ending at } \ell \\
&\quad + \text{diagram: a wavy line starting at } \ell, \text{ with an up arrow, ending at } \ell \\
&\quad + \text{diagram: a wavy line starting at } \ell, \text{ with an up arrow, ending at } \ell \\
&\quad + \dots \\
&\quad + \text{diagram: a wavy line starting at } \ell, \text{ with a down arrow, ending at } \ell \\
&\quad + \text{diagram: a wavy line starting at } \ell, \text{ with a down arrow, ending at } \ell \\
&\quad + \text{diagram: a wavy line starting at } \ell, \text{ with a down arrow, ending at } \ell \\
&\quad + \dots \\
&\quad - \text{diagram: a dashed line starting at } \ell, \text{ ending at } \ell
\end{aligned}$$

where the final $-1/(P_\ell - \gamma\beta_\ell^m)$ is to remove the double counting of $\bullet \cdots \bullet$.

We may write the sum

$$\begin{aligned}
W_\ell^{(\pm)m} &= \left(\frac{1}{P_\ell - \gamma\beta_\ell^m} \right) \sum_{n=0}^{\infty} \left[\left((P_\ell - \gamma\beta_\ell^m) W_\ell^{(+m)} - 1 \right) \left((P_\ell - \gamma\beta_\ell^m) W_\ell^{(-m)} - 1 \right) \right]^n \\
&\quad \times \left(2 + (P_\ell - \gamma\beta_\ell^m) W_\ell^{(+m)} - 1 + (P_\ell - \gamma\beta_\ell^m) W_\ell^{(-m)} - 1 \right) - \left(\frac{1}{P_\ell - \gamma\beta_\ell^m} \right) \\
&= \frac{W_\ell^{(+m)} W_\ell^{(-m)}}{W_\ell^{(-m)} - (P_\ell - \gamma\beta_\ell^m) W_\ell^{(+m)} W_\ell^{(-m)} + W_\ell^{(+m)}} \tag{50}
\end{aligned}$$

The term $W_\ell^{(\pm)m}$ gives all the diagrams starting and ending at m and ℓ . The sum of diagrams that connect different ℓ values

$$G_{\ell_0, \ell_f}^m \equiv \text{diagram: a wavy line starting at } \ell_0, \text{ ending at } \ell_f \\
\equiv \text{diagram: a wavy line starting at } \ell_0, \text{ ending at } \ell_f \\
\equiv \text{diagram: a wavy line starting at } \ell_0, \text{ ending at } \ell_f$$

can be calculated recursively

$$G_{\ell_0, \ell_f}^m = \begin{cases} 0 & \text{if } \ell_f - \ell_0 \text{ is odd} \\ W_{\ell_0}^{(\pm)m} & \text{if } \ell_f = \ell_0 \\ G_{\ell_0, \ell_f-2}^m W_{\ell_f}^{(+m)} A_{\ell_f}^m \gamma & \text{if } \ell_f > \ell_0 \\ G_{\ell_0, \ell_f+2}^m W_{\ell_f}^{(-m)} A_{\ell_f+2}^m \gamma & \text{if } \ell_f < \ell_0 \end{cases} \tag{51}$$

with the application of the flanking harmonics we have our desired propagator

$$\check{G}(\vec{u}|\vec{u}_0; p) = \sum_{\ell=0}^{\infty} \sum_{m=-\ell}^{\ell} Y_{\ell,m}(\vec{u}_0) G_{\ell_0 \ell_f}^m Y_{\ell,m}(\vec{u}) \quad (52)$$

VIII. EVALUATING EXPECTATIONS

In this section we will show how the propagator \check{G} can be used to calculate expectation values of various quantities (e.x. $\langle \phi_{2,0} \rangle^{MF}$ or $\langle \phi_{2,1} \phi_{2,1} \rangle^{MF}$) for WLC's in an aligning mean field.

In the mean field solution, the n_p polymers are distributed over a volume \mathcal{V} . Taking the expectation value of equation 7 we have

$$\langle \phi_{2,0} \rangle^{MF} = \left\langle n_p \frac{1}{\mathcal{V}} A \sqrt{\frac{4\pi}{5}} 2\ell_p \int_0^N ds Y_{2,0}(\vec{u}(s)) \right\rangle^{MF} \quad (53)$$

or

$$\langle \phi_{2,0} \rangle^{MF} = \sqrt{\frac{4\pi}{5}} \frac{\phi_{0,0}}{N} \int_0^N ds \langle Y_{2,0}(\vec{u}(s)) \rangle^{MF} \quad (54)$$

The probability the chain will point in direction \vec{u} at path length s along the chain is weighted by the propagator from the beginning of the chain to s , i.e. $G(\vec{u}|\vec{u}_0; s)$, and the propagator from s to the other end of the chain $G(\vec{u}_f|\vec{u}; L-s)$. The Laplace transform from N to p of $\langle \phi_{2,0} \rangle^{MF}$ can be preformed using the convolution rule (see discussion of equation 44)

$$\mathcal{L} \left[\int_0^N ds G(\vec{u}_f|\vec{u}; p) G(\vec{u}|\vec{u}_0; s) \right] = \check{G}(\vec{u}_1|\vec{u}_0; p) \check{G}(\vec{u}_f|\vec{u}_1; p) \quad (55)$$

To calculate $\langle \phi_{2,0} \rangle^{MF}$ we want to integrate over beginning, middle, and end orientations as in

$$\langle \phi_{2,0} \rangle^{MF} = \frac{\phi_{0,0}}{N} \sqrt{\frac{4\pi}{5}} \frac{\mathcal{L}^{-1} \left[\int du_0 \int du_1 \int du_f \check{G}(\vec{u}_1|\vec{u}_0; p) Y_{2,0}(\vec{u}_1) \check{G}(\vec{u}_f|\vec{u}_1; p) \right] (N)}{\mathcal{L}^{-1} \left[\int du_0 \int du_f \check{G}(\vec{u}_f|\vec{u}_0; p) \right] (N)} \quad (56)$$

where the denominator provides the appropriate normalization. We can then substitute equation 52 into 56 to change basis from \vec{u} to $Y_{\ell,m}$. The sums over ℓ can be made implicit by writing the result in matrix form where the rows and columns run over ℓ values so that

$$(\mathbf{G}^m)_{\ell_1, \ell_2} = G_{\ell_0 \ell_f}^m \quad (57)$$

and the product of three real spherical harmonics is defined as

$$\left(\mathbf{J}_{(\ell)}^{m, m', m''} \right)_{\ell_1, \ell_2} \equiv \int d\vec{u} Y_{\ell_1, m}(\vec{u}) Y_{\ell, m'}(\vec{u}) Y_{\ell_2, m''}(\vec{u}) \quad (58)$$

The values of $\mathbf{J}_{(\ell)}^{m, m', m''}$ are derived in appendix A. After the change of basis, equation 56 becomes

$$\phi_{2,0}^{MF} = \frac{\phi_{0,0}}{N} \sqrt{\frac{4\pi}{5}} \frac{\mathcal{L}^{-1} \left[\mathbf{e}_0 \cdot \mathbf{G}^0 \cdot \mathbf{J}_{(2)}^{0,0,0} \cdot \mathbf{G}^0 \cdot \mathbf{e}_0 \right] (N)}{\mathcal{L}^{-1} [\mathbf{e}_0 \cdot \mathbf{G}^0 \cdot \mathbf{e}_0] (N)} \quad (59)$$

were $\mathbf{e}_0 = [1, 0, 0, 0 \dots]$ is the unit vector so that $\mathbf{e}_0 \cdot \mathbf{G}^0 \cdot \mathbf{e}_0 = \mathbf{G}_{1,1}^0$. The pinning to $\ell = 0$ at the chain ends results from inserting $Y_{0,0} = \frac{1}{\sqrt{4\pi}}$ and applying $\int d\vec{u} Y_{0,0} Y_{\ell,m} = \delta_{0,\ell} \delta_{0,m}$. Furthermore, the requirement that $|m| \leq \ell$ required $m_1 = m_2 = 0$ in equation 59. The inverse Laplace transforms can be performed numerically as described in section XVI.

The process of connecting sequential propagators together can be extended to the expectation value of several spherical harmonics

$$\frac{\int_0^N ds_n \dots \int_0^{s_2} ds_1 \left\langle \prod_{j=1}^n Y_{\ell_j, m_j}(s_j) \right\rangle^{MF}}{\mathcal{L}^{-1} [e_0 \cdot \mathbf{G}^0 \cdot e_0]} = \dots \quad (60)$$

$$\mathcal{L}^{-1} \left[\sum_{\mathcal{M}, \dots, \mathcal{M}'''} e_0 \cdot \mathbf{G}^0 \cdot \mathbf{J}_{(\ell_n)}^{0, m_n, \mathcal{M}} \cdot \mathbf{G}^{\mathcal{M}} \cdot \mathbf{J}_{(\ell_{n-1})}^{\mathcal{M}, m_{n-1}, \mathcal{M}'} \cdot \dots \cdot \mathbf{G}^{\mathcal{M}'''} \cdot \mathbf{J}_{(\ell_1)}^{\mathcal{M}''', m_1, 0} \cdot \mathbf{G}^0 \cdot e_0 \right]$$

IX. FLUCTUATIONS

Having solved for the average field values $\langle \phi \rangle^{MF}$ (and by extension $W_1^{MF} = -iV_{12} \langle \phi \rangle_2^{MF}$) we now investigate local fluctuations about these values by substituting $\phi = \langle \phi \rangle^{MF} + \delta\phi$ and $W = W^{MF} + \delta W$ into 19. Resulting constant terms such as $W^{MF} \langle \phi \rangle^{MF}$ can be absorbed into the proportionality constant which only offsets the reference energy. Furthermore, the mean field solution W^{MF} found above was uniform in space so the term $W_1^{MF} \delta\phi_1$ must be zero. Equation 19 can further be simplified by using $iW_1^{MF} = V_{12} \langle \phi \rangle_2^{MF}$ yielding:

$$Z \propto \int \mathcal{D}\delta W \delta\phi \exp \left[-\frac{1}{2} \delta\phi_1 V_{12} \delta\phi_2 + i\delta W_1 \delta\phi_1 + n_p \log(z_p) \right] \quad (61)$$

$$z_p = \int \mathcal{D}r_i^{(1)} \exp \left[-\beta E_{poly} - \hat{\phi}_1^{(1)} V_{12} \langle \phi \rangle_2^{MF} - i\delta W_1 \hat{\phi}_1^{(1)} \right] \quad (62)$$

Per assumption 12, the field ϕ only makes small deviations from its mean field value $\langle \phi \rangle^{MF}$ so $\delta\phi$ is small. Also, under RPA (assumption 13) W only makes small deviations from its mean value W^{MF} constraining δW to be small. Taylor expanding z_p about $\delta W = 0$ gives

$$z_p \approx 1 + \left\langle -i\delta W_1 \hat{\phi}_1^{(1)} \right\rangle^{MF} + \frac{1}{2} \left(\left\langle -i\delta W_1 \hat{\phi}_1^{(1)} \right\rangle^{MF} \right)^2 \quad (63)$$

(up to an additive constant of no consequence). We expand the logarithm $\log(1+x) = x - \frac{1}{2}x^2$ in equation 61 and substituting in z_p we have

$$Z \propto \int \mathcal{D}W \delta\phi e^{-\frac{1}{2} \delta\phi_1 V_{12} \delta\phi_2 + i\delta W_1 \delta\phi_1 - n_p \frac{1}{2} \delta W_1 S_{12} \delta W_2} \quad (64)$$

where

$$S_{12} \equiv \left\langle \hat{\phi}_1^{(1)} \hat{\phi}_2^{(1)} \right\rangle^{MF} - \left\langle \hat{\phi}_1^{(1)} \right\rangle^{MF} \left\langle \hat{\phi}_2^{(1)} \right\rangle^{MF}. \quad (65)$$

We then perform a Gaussian integral over δW to arrive at

$$Z \propto \int \mathcal{D}\delta\phi \exp \left[-\frac{1}{2} \delta\phi_1 \left(V_{12} + \frac{1}{n_p} S_{12}^{-1} \right) \delta\phi_2 \right] \quad (66)$$

where S_{12}^{-1} is defined via $S_{12}^{-1} S_{23} = \delta_{\ell_1, \ell_3} \delta_{m_1, m_3} \delta(\vec{r}_1 - \vec{r}_3)$. Appendix C discusses how to perform this inverse.

The energy expression in 66, which is often written with $\Gamma_{12} \equiv V_{12} + \frac{1}{n_p} S_{12}^{-1}$, describes the quadratic fluctuations of ϕ around the mean field solution. The bigger an element of Γ is, the smaller the corresponding fluctuation will be. Given the critical importance of 66 we will devote considerable effort to calculating S^{-1} .

Because of translational invariance (assumption 7), the Fourier transform $\vec{r} \rightarrow \vec{k}$ of S_{12} is much easier to invert than the real space S_{12} . Following the conventions in appendix B,

$$Z \propto \int \mathcal{D}\tilde{\phi} \exp \left[-\frac{1}{2} \delta\tilde{\phi}_1 \left(\tilde{V}_{12} + \frac{1}{n_p} \tilde{S}_{12}^{-1} \right) \delta\tilde{\phi}_2 \right] \quad (67)$$

where $\tilde{V}_{12} = (4\pi\chi\delta_{\ell_1,0} - \frac{8\pi}{15}a\delta_{\ell_1,2})\delta_{m_1,m_2}\delta_{\ell_1,\ell_2}\delta(\vec{k}_1 + \vec{k}_2)$. In other words, the Fourier modes of fluctuations in ϕ are decoupled from each other (at least to quadratic order in ϕ). Another advantage of the Fourier transform is that by assumptions 7, 8, and 12 and as discussed in section VI the mean field solution is uniform in space so the latter term in equation 65, $\langle \hat{\phi}_1^{(1)} \rangle^{MF} \langle \hat{\phi}_2^{(1)} \rangle^{MF}$, contributes only at $\vec{k} = 0$. While we will be interested in the limit as $\vec{k} \rightarrow 0$, the value at precisely $\vec{k} = 0$ will not be used so we can drop this constant term. We will refer to the first term on the right of equation 65 as $\delta S_{12} \equiv \langle \hat{\phi}_1^{(1)} \hat{\phi}_2^{(1)} \rangle^{MF}$.

X. CALCULATING S FOR FUZZBALL AND RIGID ROD

Calculating δS for a fuzzball or rigid rod can be accomplished using \mathbf{M} from equation 27 which amounts to the expectation of a product of two spherical harmonics in an applied field. Inserting equation 13 into $\delta S_{12} \equiv \langle \hat{\phi}_1^{(1)} \hat{\phi}_2^{(1)} \rangle^{MF}$ for the fuzzball the spatial and rotational terms, ρ and v respectively, factor because the position and orientation of a fuzzball are unrelated.

$$\delta \tilde{S}_{12}^{FB} = \rho(\vec{r}_1, \vec{r}_2) v(\ell_1, m_1, \ell_2, m_2) \quad (68)$$

$$\rho(\vec{r}_1, \vec{r}_2) = \frac{1}{\mathcal{V}} \int d\vec{r}_i \frac{v_p^2}{(2\pi\sigma^2)^3} \exp \left(-\frac{(\vec{r}_1 - \vec{r}_i)^2}{2\sigma^2} - \frac{(\vec{r}_2 - \vec{r}_i)^2}{2\sigma^2} \right) \quad (69)$$

$$v(\ell_1, m_1, \ell_2, m_2) = \frac{4\pi}{\sqrt{(2\ell_1+1)(2\ell_2+1)}} \frac{\mathbf{M}_{\ell_1, \ell_2}^{m_1} \delta_{m_1, m_2}}{4\pi \mathbf{M}_{0,0}^0} \quad (70)$$

where the denominators come from the single fuzzball partition function $z^{FB} = \mathcal{V} \int d\vec{u} \exp(\gamma Y_{2,0}(\vec{u}_i)) = \mathcal{V} 4\pi M_{0,0}^0$. Taking the Fourier transform of a Gaussian yields a Gaussian, hence

$$\delta \tilde{S}_{12}^{FB} = \frac{v_p^2}{\mathcal{V}} \delta(\vec{k}_1 + \vec{k}_2) e^{-\sigma^2 \vec{k}^2} \frac{\mathbf{M}_{\ell_1, \ell_2}^{m_1} \delta_{m_1, m_2}}{\sqrt{(2\ell_1+1)(2\ell_2+1)} \mathbf{M}_{0,0}^0} \quad (71)$$

where the $\delta(\vec{k}_1 + \vec{k}_2)$ arises from translational invariance.

The position along a rigid rod is inherently coupled to the orientation of the rod so the factorization into ρ and v is not possible. In particular, writing out $\delta \tilde{S} = \langle \hat{\phi}_1^{(1)} \hat{\phi}_2^{(1)} \rangle^{MF}$ explicitly from equation IV we have

$$\begin{aligned} \delta S_{12}^{RR} &= \frac{1}{z^{RR}} \frac{A^2}{\sqrt{(2\ell_1+1)(2\ell_2+1)}} \\ &\times \int d\vec{r}_j \int d\vec{u}_j e^{\gamma Y_{2,0}(\vec{u}_j)} \int_0^L ds_1 \delta(\vec{r}_j + s_1 \vec{u}_j - \vec{r}_1) \int_0^L ds_2 \delta(\vec{r}_j + s_2 \vec{u}_j - \vec{r}_2) Y_{\ell_1, m_1}(\vec{u}_j) Y_{\ell_2, m_2}(\vec{u}_j) \end{aligned} \quad (72)$$

where the single rod partition function is $z^{RR} = \mathcal{V} \int d\vec{u} \exp(\gamma Y_{2,0}(\vec{u}_i)) = \mathcal{V} 4\pi \mathbf{M}_{0,0}^0$. Applying the Fourier transform from $\vec{r} \rightarrow \vec{k}$ takes

$$\delta(\vec{r}_j + s_1 \vec{u}_j - \vec{r}_1) \delta(\vec{r}_j + s_2 \vec{u}_j - \vec{r}_2) \rightarrow \delta(\vec{k}_1 + \vec{k}_2) \exp(i\vec{k} \cdot \vec{u}_j (s_1 - s_2)). \quad (73)$$

The exponential can be expanded to quadratic order and the s integrals evaluated directly

$$\int_0^L ds_1 \int_0^L ds_2 \exp(i\vec{k} \cdot \vec{u}_j (s_1 - s_2)) \approx L^2 - \frac{1}{2} (\vec{k} \cdot \vec{u}_j)^2 \frac{L^4}{6}. \quad (74)$$

Introducing κ defined in equation 79 and doing some simplification we arrive at

$$\delta\tilde{S}_{12}^{RR} = \frac{A^2 \delta(\vec{k}_1 + \vec{k}_2)}{\sqrt{(2\ell_1 + 1)(2\ell_2 + 1)}} \left[\frac{L^2}{\mathcal{V}} \frac{\mathbf{M}_{\ell_1, \ell_2}^{m_1}}{\mathbf{M}_{0,0}^0} \delta_{m_1, m_2} - \frac{4\pi}{z^{RR}} \frac{L^4}{12} \sum_{m=-1}^1 \sum_{m'=-1}^1 \kappa_{1,m} \kappa_{1,m'} \sum_{\mathcal{M}} \left(\mathbf{J}_{(1)}^{m_1, m, \mathcal{M}} \cdot \mathbf{M}^{\mathcal{M}} \cdot \mathbf{J}_{(1)}^{\mathcal{M}, m', m_2} \right)_{\ell_1, \ell_2} \right] \quad (75)$$

where the integer \mathcal{M} runs over all values allowed by the selection rules of \mathbf{J} . We now have an explicit formula for the low k expansion of $\delta\tilde{S}^{RR}$.

XI. CALCULATING S FOR WLC

We now turn to finding δS_{12} for the WLC. Writing δS_{12} explicitly

$$(\delta S_{12})_{\ell_1 \ell_2}^{m_1 m_2}(\vec{r}_1, \vec{r}_2) = \frac{4\pi}{\sqrt{(2\ell_1 + 1)(2\ell_2 + 1)}} A^2 \int_0^L ds_2 \int_0^L ds_1 \langle Y_{\ell_1, m_1}(\vec{u}(s_1)) \delta(\vec{r}_1 - \vec{r}(s_1)) Y_{\ell_2, m_2}(\vec{u}(s_2)) \delta(\vec{r}_2 - \vec{r}(s_2)) \rangle^{MF} \quad (76)$$

Note the distinction between the argument \vec{r}_1 and the unitalicized $\vec{r}(s_1)$ which stands for position of a point s_1 along the polymer. We take the Fourier transform $\vec{r}_1 \rightarrow \vec{k}_1$ and $\vec{r}_2 \rightarrow \vec{k}_2$ via $\frac{1}{(2\pi)^3} \int d\vec{r}_1 d\vec{r}_2 \exp(i\vec{k}_1 \vec{r}_1 + i\vec{k}_2 \vec{r}_2)$. The integrals over \vec{r} are eliminated by delta functions to give $\exp(i\vec{k}_1 \vec{r}(s_1) + i\vec{k}_2 \vec{r}(s_2))$ which can be factored into $\exp[i\vec{k}_1 \cdot (\vec{r}_1 - \vec{r}_2)] \exp[i(\vec{k}_1 + \vec{k}_2) \cdot \vec{r}_2]$ where we have introduced the notation $\vec{r}(s_2) = \vec{r}_2$. By translational invariance (assumption 7) we can average out \vec{r}_2 over the system volume \mathcal{V} by applying $\mathcal{V}^{-1} \int d\vec{r}_2$ and recognizing the delta function $(2\pi)^3 \delta(\vec{k}_1 + \vec{k}_2) = \int d\vec{r} e^{i\vec{r}(\vec{k}_1 + \vec{k}_2)}$, giving

$$\delta\tilde{S}_{12} = \frac{4\pi}{\sqrt{(2\ell_1 + 1)(2\ell_2 + 1)}} \frac{A^2 (2\ell_p)^2}{\mathcal{V}} \delta(\vec{k}_1 + \vec{k}_2) \int_0^N ds_2 \int_0^N ds_1 \langle Y_{\ell_1, m_1}(\vec{u}_1) \exp[i\vec{k}_1 \cdot (\vec{r}_1 - \vec{r}_2)] Y_{\ell_2, m_2}(\vec{u}_2) \rangle^{MF} \quad (77)$$

where we nondimensionalized $L = \frac{N}{2\ell_p}$ so that $\int_0^L ds_2$ became $2\ell_p \int_0^N ds_2$. It will be convenient to write \vec{k} in spherical coordinates. Because \vec{k} is a vector, it is an $\ell = 1$ object. Specifically we will define $\kappa_{\ell, m}$ as

$$\kappa_{1, m} \equiv \sqrt{\frac{4\pi}{3}} \begin{cases} k_y & m = -1 \\ k_z & m = 0 \\ k_x & m = 1 \end{cases} \quad (78)$$

which has the property

$$\vec{k} \cdot \vec{u} = \sum_{m=-1}^1 \kappa_{1, m} Y_{1, m}(\vec{u}) \quad (79)$$

which is useful because $\vec{k}_1 \cdot (\vec{r}_1 - \vec{r}_2)$ in equation 77 can be written as $\vec{k}_1 \cdot (2\ell_p) \int_{s_1}^{s_2} ds \vec{u}(s) = \int_{s_1}^{s_2} ds \sum_{m=-1}^1 \kappa'_{1, m} Y_{1, m}(\vec{u})$ where $\kappa' = 2\ell_p \kappa$. It can be shown – or verified numerically – that $\int_0^N ds_2 \int_0^N ds_1$ may be replaced with $2 \int_0^N ds_2 \int_0^{s_2} ds_1$ in this expression. To further simplify the expression we define the nondimensionalized

$$\tilde{S}'_{12}(\vec{k}) \equiv \delta\tilde{S}_{12}(\vec{k}_1, -\vec{k}_1) \frac{\mathcal{V}}{A^2 (2\ell_p)^2 N^2} \quad (80)$$

By assumption 15 we are interested in the large distance (small \vec{k}) behavior, so we Taylor expand the exponential in 77 which, along with the above modifications, becomes

$$\begin{aligned}
\tilde{S}'_{12} \approx & \frac{4\pi}{\sqrt{(2\ell_1+1)(2\ell_2+1)}} \frac{2}{N^2} \\
& \times \left[\int_0^N ds_2 \int_0^{s_2} ds_1 \langle Y_{\ell_1, m_1}(\vec{u}_1) Y_{\ell_2, m_2}(\vec{u}_2) \rangle^{MF} \right. \\
& + \sum_{m=-1}^1 i\kappa'_{1,m} \int_0^N ds_3 \int_0^{s_3} ds_2 \int_0^{s_2} ds_1 \langle Y_{\ell_1, m_1}(\vec{u}_1) Y_{1,m}(\vec{u}_2) Y_{\ell_2, m_2}(\vec{u}_3) \rangle^{MF} \\
& \left. - \sum_{m, m'=-1}^1 \kappa'_{1,m} \kappa'_{1,m'} \int_0^N ds_4 \int_0^{s_4} ds_3 \int_0^{s_3} ds_2 \int_0^{s_2} ds_1 \langle Y_{\ell_1, m_1}(\vec{u}_1) Y_{1,m}(\vec{u}_2) Y_{1,m'}(\vec{u}_3) Y_{\ell_2, m_2}(\vec{u}_4) \rangle^{MF} \right] \quad (81)
\end{aligned}$$

The expectation values in 81 can be evaluated as described in equation 60. The first term in the series becomes

$$\int_0^N ds_2 \int_0^{s_2} ds_1 \langle Y_{\ell_1, m_1}(\vec{u}_1) Y_{\ell_2, m_2}(\vec{u}_2) \rangle^{MF} = \frac{\mathcal{L}^{-1} \left[\mathbf{e}_0 \cdot \mathbf{G}^0 \cdot \mathbf{J}_{(\ell_1)}^{0, m_1, m_1} \cdot \mathbf{G}^{m_1} \cdot \mathbf{J}_{(\ell_2)}^{m_1, m_1, 0} \cdot \mathbf{G}^0 \cdot \mathbf{e}_0 \right] \delta_{m_1, m_2}}{\mathcal{L}^{-1} [\mathbf{e}_0 \cdot \mathbf{G}^0 \cdot \mathbf{e}_0]} \quad (82)$$

the linear term is killed by selection rules for \mathbf{J} and the quadratic term is given by

$$\begin{aligned}
& \int_0^N ds_4 \int_0^{s_4} ds_3 \int_0^{s_3} ds_2 \int_0^{s_2} ds_1 \langle Y_{\ell_1, m_1}(\vec{u}_1) Y_{1,m}(\vec{u}_2) Y_{1,m'}(\vec{u}_3) Y_{\ell_2, m_2}(\vec{u}_4) \rangle^{MF} \\
& = \frac{\mathcal{L}^{-1} \left[\sum_{\mathcal{M}} \mathbf{e}_0 \cdot \mathbf{G}^0 \cdot \mathbf{J}_{(\ell_1)}^{0, m_1, m_1} \cdot \mathbf{G}^{m_1} \cdot \mathbf{J}_{(1)}^{m_1, m, \mathcal{M}} \cdot \mathbf{G}^{\mathcal{M}} \cdot \mathbf{J}_{(1)}^{\mathcal{M}, m', m_2} \cdot \mathbf{G}^{m_2} \cdot \mathbf{J}_{(\ell_2)}^{m_2, m_2, 0} \cdot \mathbf{G}^0 \cdot \mathbf{e}_0 \right]}{\mathcal{L}^{-1} [\mathbf{e}_0 \cdot \mathbf{G}^0 \cdot \mathbf{e}_0]}. \quad (83)
\end{aligned}$$

XII. CANCELLATION

Having gone through the effort to calculate the low k behavior of $\delta\tilde{S}$ it is worth taking some time to consider the form of the result. In this paper we are primarily interested in the density $\ell = 0$ and quadrupole $\ell = 2$ interactions. It is convenient to write $\delta\tilde{S}$ in the basis

$$(\ell_i, m_i) = [(0, 0), (2, 0), (2, -1), (2, 1), (2, -2), (2, 2)]. \quad (84)$$

In the long wavelength limit there are only correlations between fluctuations of the same m values, i.e. $\lim_{k \rightarrow 0} \delta\tilde{S} \propto \delta_{m_1, m_2}$. As it turns out, in this basis we have

$$\lim_{\vec{k} \rightarrow 0} \delta\tilde{S}_{\ell_1 \ell_2}^{m_1, m_2} = \begin{bmatrix} t & h & 0 & 0 & 0 & 0 \\ h & x & 0 & 0 & 0 & 0 \\ 0 & 0 & y & 0 & 0 & 0 \\ 0 & 0 & 0 & y & 0 & 0 \\ 0 & 0 & 0 & 0 & z & 0 \\ 0 & 0 & 0 & 0 & 0 & z \end{bmatrix} \quad (85)$$

where the expressions for t , h , x , y , and z depend on whether we are talking about a WLC, rigid rod, or fuzball. In section XIII we will discuss the meaning of the various fluctuations (see equation 101 and figure 6). For now, we will point out that t governs density-density interactions, x governs variations in alignment strength, y governs variations in alignment direction, and z governs fluctuations in a secondary direction of alignment. As the Frank elastic constants are of most interest to us we will focus on y . Here we provide plots of $\lim_{\vec{k} \rightarrow 0} \delta\tilde{S}_{\ell_1 \ell_2}^{m_1, m_2}$ for a nearly rigid WLC.

In the isotropic limit, $\gamma \rightarrow 0$, all directions $Y_{2,m}$ are identical. As alignment in the \hat{z} direction (i.e. $Y_{2,0}$) grows, it does so at the expense of the alignment in the other directions.

When $\delta\tilde{S}$ is inverted and substituted into equation 66 we get the energy coefficients

$$\tilde{\Gamma}_{12} = \left(\chi \delta_{\ell_1, 0} - \frac{2}{3} a \delta_{\ell_1, 2} \right) \delta_{m_1, m_2} \delta_{\ell_1, \ell_2} \delta(\vec{k}_1 + \vec{k}_2) + \frac{1}{n_p} \delta\tilde{S}_{12}^{-1} \quad (86)$$

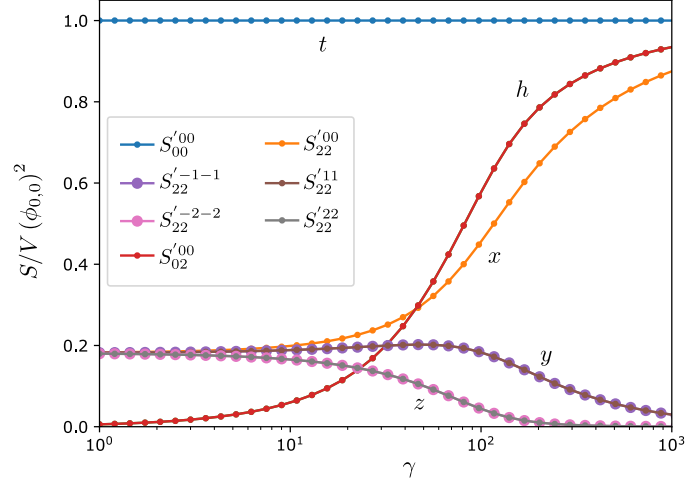


FIG. 4. Plot of selected terms of $\lim_{k \rightarrow 0} \delta \tilde{S}$ as a function of field strength. Because $\lim_{k \rightarrow 0} \delta \tilde{S}_{2,2}^{1,1} = \lim_{k \rightarrow 0} \delta \tilde{S}_{2,2}^{-1,-1}$ and $\lim_{k \rightarrow 0} \delta \tilde{S}_{2,2}^{2,2} = \lim_{k \rightarrow 0} \delta \tilde{S}_{2,2}^{-2,-2}$ some curves are the same.

for the various modes where the inverse is discussed in C. Critically, we have verified numerically, that in the limit that $\tilde{\kappa} \rightarrow 0$ that y precisely cancels with $\frac{2}{3}a$ term from the original interaction potential. This cancellation occurs at all field strengths γ . This cancellation comes about because of the invariance of the energy to a rotation of the entire system. Hence, the system will exhibit long distance deformations in the direction of alignment. It is only the rate of change of these directions that contribute to the energy, hence the derivatives, ∇ , in the Frank elastic expressions.

XIII. FRANK ELASTIC ENERGIES

In this section we will define the nematic director and Frank elastic constants and their relation to the orientation field $\hat{\phi}$. The Frank elastic energy density depends on the orientations \vec{u} in the vicinity ΔV . The orientation distribution can be described by the 3x3 matrix

$$M = \frac{\int^{\Delta V} d\vec{r} \sum_{j=1}^{n_p} A \int_0^L ds \delta(\vec{r} - \vec{r}_j(s)) \vec{u}_j(s) \otimes \vec{u}_j(s)}{\int^{\Delta V} d\vec{r} \sum_{j=1}^{n_p} A \int_0^L ds \delta(\vec{r} - \vec{r}_j(s))} \quad (87)$$

the denominator of which normalizes out the local polymer density, $\phi_{0,0}$, leaving only the directional information. The ΔV is the coarse-graining volume such that details of the structure smaller than this volume will not be treated. Going forward we will drop the $\int^{\Delta V}$. The eigen-decomposition of the M matrix is [29]

$$M = \lambda_1 \vec{n} \otimes \vec{n} + \lambda_2 \vec{e}_2 \otimes \vec{e}_2 + \lambda_3 \vec{e}_3 \otimes \vec{e}_3 \quad (88)$$

where $\lambda_1 \geq \lambda_2 \geq \lambda_3$. This defines the unit length nematic director \vec{n} which indicates the general direction of alignment within ΔV . As \vec{n} is an eigenvector, its sign is arbitrarily chosen. The eigenvalues of M , which obey $\lambda_1 + \lambda_2 + \lambda_3 = 1$ and $\lambda_i \geq 0$, designate the degree of alignment [29]. The interpretation of λ_i can be understood in terms of the traceless alignment matrix

$$Q \equiv M - \frac{1}{3} I c_1 = c_1 \left(\vec{n} \otimes \vec{n} - \frac{1}{3} I \right) + c_2 (\vec{e}_2 \otimes \vec{e}_2 - \vec{e}_3 \otimes \vec{e}_3) \quad (89)$$

where

$$c_1 = \frac{3\lambda_1 - 1}{2}, \quad c_2 = \lambda_2 - \lambda_1 \quad (90)$$

with $c_1 \in [0, 1]$ describing the degree of alignment in the primary direction and c_2 describing the degree to which a secondary direction of alignment exists.

The Frank elastic energy density is the sum of bend, twist, and splay energies and is defined in terms of the nematic director

$$E_{Frank} = \frac{1}{2}K_{bend} \langle (\vec{n} \times \nabla \times \vec{n})^2 \rangle + \frac{1}{2}K_{twist} \langle (\vec{n} \cdot \nabla \times \vec{n})^2 \rangle + \frac{1}{2}K_{splay} \langle (\nabla \cdot \vec{n})^2 \rangle \quad (1 \text{ revisited})$$

To see why there are exactly three deformation modes, consider figure 5. Each mode prescribes a change in orientation associated with a displacement. For each mode there is a direction \vec{n} of alignment (represented by the cylinder), a displacement (green arrow), and a change in the direction of alignment (red arrow). The displacement must be perpendicular to \vec{n} as it is a differential change. The displacement, therefore, can be in one of three direction: 1) parallel to \vec{n} , in which case the deformation is bend; 2) parallel to the change in direction, in which case the deformation is splay; and 3) perpendicular to both, in which case the deformation is twist.



FIG. 5. Pictorial representation clarifying the chief difference between bend, twist, and splay. The axes of the cylinders represent the direction of nematic ordering, \vec{n} . Each green arrow represents a displacement to a different position in a liquid crystal. Red arrows represent the change in orientation associated with the change in position. A semitransparent cylinder represents the new position but with the old orientation as a guide to the eye.

We will devote the remainder of this derivation to finding the Frank elastic constants K_{bend} , K_{twist} , and K_{splay} in terms of polymer properties. Our first goal will be to solve for the associated expectation values in terms of $\hat{\phi}_{\ell,m}$. We begin by exploring the relation between $\hat{\phi}$ and $\vec{u}_j(s) \otimes \vec{u}_j(s)$. Using the real spherical harmonic for $\ell = 2$

$$Y_{2,m}(\vec{u}) = \sqrt{\frac{5}{4\pi}} \begin{cases} \sqrt{3}u_xu_y & m = -2 \\ \sqrt{3}u_yu_z & m = -1 \\ \frac{1}{2}(3u_z^2 - 1) & m = 0 \\ \sqrt{3}u_zu_x & m = 1 \\ \frac{\sqrt{3}}{2}(u_x^2 - u_y^2) & m = 2 \end{cases} \quad (91)$$

and definition 7 we can write

$$Q = \frac{1}{\phi_{0,0}} \sum_{j=1}^{n_p} A \int_0^L ds \delta(\vec{r} - \vec{r}_j(s)) \left(\vec{u}_j(s) \otimes \vec{u}_j(s) - \frac{1}{3}\mathbb{I} \right) \quad (92)$$

$$= \frac{1}{\phi_{0,0}\sqrt{3}} \begin{bmatrix} \hat{\phi}_{2,2} - \frac{1}{\sqrt{3}}\hat{\phi}_{2,0} & \hat{\phi}_{2,-2} & \hat{\phi}_{2,1} \\ \hat{\phi}_{2,-2} & -\hat{\phi}_{2,2} - \frac{1}{\sqrt{3}}\hat{\phi}_{2,0} & \hat{\phi}_{2,-1} \\ \hat{\phi}_{2,1} & \hat{\phi}_{2,-1} & \frac{2}{\sqrt{3}}\hat{\phi}_{2,0} \end{bmatrix} \quad (93)$$

The magnitude of $\hat{\phi}_{2,m}$ integrated over a coarse-graining volume ΔV depends on the direction and degree of local alignment of \vec{u} vectors and grows with amount of polymer within ΔV .

Explicitly writing the relation between \hat{n} and $\hat{\phi}_{2,m}$ is complicated as it involves the cubic equation for the eigenvalues of M . This relation can be much simplified by first making some assumptions. By assumption 19, there is a primary direction of alignment requiring $\lambda_1 > \lambda_2$ implying $c_1 > 0$. Furthermore, assumption 12 requires the direction of alignment to be approximately in the \hat{z} direction. Excluding terms that are quadratic in the deviation from \hat{z} (i.e. of order $n_{x/y}^2$ or higher) we write

$$\vec{n} \approx \hat{z} + n_x\hat{x} + n_y\hat{y} \quad (94)$$

$$\vec{e}_2 \approx (\hat{x} - n_x \hat{z}) \cos(\theta) + (\hat{y} - n_y \hat{z}) \sin(\theta) \quad (95)$$

$$\vec{e}_3 \approx (\hat{y} - n_y \hat{z}) \cos(\theta) - (\hat{x} - n_x \hat{z}) \sin(\theta) \quad (96)$$

where θ specifies the orientation of any azimuthal asymmetry. Substituting into 89

$$\vec{e}_2 \approx \cos(\theta) \hat{x} + \sin(\theta) \hat{y} - (n_y \sin(\theta) + n_x \cos(\theta)) \hat{z} \quad (97)$$

$$\vec{e}_3 \approx -\sin(\theta) \hat{x} + \cos(\theta) \hat{y} + (-n_y \cos(\theta) + n_x \sin(\theta)) \hat{z} \quad (98)$$

and

$$Q = \begin{bmatrix} -\frac{1}{3}c_1 + c_2 \cos 2\theta & c_2 \sin 2\theta & c_1 n_x - c_2 (\sin 2\theta n_y + \cos 2\theta n_x) \\ - & -\frac{1}{3}c_1 - c_2 \cos 2\theta & c_1 n_y + c_2 (\cos 2\theta n_y - \sin 2\theta n_x) \\ - & - & \frac{2}{3}c_1 \end{bmatrix} \quad (99)$$

where the dashes indicate a symmetric matrix.

By assumption 14 we will work with systems where $c_2 \approx 0$ and therefore $\lambda_2 \approx \lambda_3 \approx (1 - \lambda_1)/2$. We write c_1 and c_2 in terms of their deviations so that $c_1 \rightarrow c_1 + \delta c_1$ and $c_2 \rightarrow 0 + \delta c_2$. Keeping only first order terms we have

$$Q = \begin{bmatrix} -\frac{1}{3}(c_1 + \delta c_1) + \delta c_2 \cos(2\theta) & \delta c_2 \sin(2\theta) & c_1 n_x \\ - & -\frac{1}{3}(c_1 + \delta c_1) - \delta c_2 \cos(2\theta) & c_1 n_y \\ - & - & \frac{2}{3}(c_1 + \delta c_1) \end{bmatrix} \quad (100)$$

Comparing to equation 93 we have

$$\hat{\phi}_{2,m} = \phi_{0,0} \begin{cases} \sqrt{3}\delta c_2 \sin(2\theta) & m = -2 \\ \sqrt{3}c_1 n_y & m = -1 \\ c_1 + \delta c_1 & m = 0 \\ \sqrt{3}c_1 n_x & m = 1 \\ \sqrt{3}\delta c_2 \cos(2\theta) & m = 2 \end{cases} \quad (101)$$

This gives us an interpretation of $\phi_{2,m}$ under the assumption that alignment only slightly differs from the \hat{z} direction as shown in figure 6. The value of $\phi_{2,0}$ dictates the magnitude of alignment, $\phi_{2,1}$ and $\phi_{2,-1}$ denote fluctuations that rotate the direction of the alignment into the \hat{x} and \hat{y} directions respectively. Meanwhile $\phi_{2,-2}$ and $\phi_{2,2}$ denote fluctuations that create a secondary direction of alignment in the \hat{x} and \hat{y} directions respectively.

Solving for \hat{n} we have

$$\vec{n} = \frac{1}{\phi_{0,0}\sqrt{3}c_1} \phi_{2,1} \hat{x} + \frac{1}{\phi_{0,0}\sqrt{3}c_1} \phi_{2,-1} \hat{y} + \hat{z} \quad (102)$$

from which we can write the bend, twist and splay

$$(\hat{n} \times \nabla \times \hat{n})^2 = \left(\frac{1}{\phi_{0,0}\sqrt{3}c_1} \right)^2 \left(\left(\frac{\partial}{\partial z} \phi_{2,1} \right)^2 + \left(\frac{\partial}{\partial z} \phi_{2,-1} \right)^2 \right) \quad (103)$$

$$(\hat{n} \cdot \nabla \times \hat{n})^2 = \left(\frac{1}{\phi_{0,0}\sqrt{3}c_1} \right)^2 \left(\frac{\partial}{\partial x} \phi_{2,-1} - \frac{\partial}{\partial y} \phi_{2,1} \right)^2 \quad (104)$$

$$(\nabla \cdot \hat{n})^2 = \left(\frac{1}{\phi_{0,0}\sqrt{3}c_1} \right)^2 \left(\frac{\partial}{\partial x} \phi_{2,1} + \frac{\partial}{\partial y} \phi_{2,-1} \right)^2 \quad (105)$$

In appendix B we show that

$$\int dx \left(\frac{\partial}{\partial x} \phi \right)^2 = \int k^2 \tilde{f}(k) \tilde{f}(-k) dk \quad (106)$$

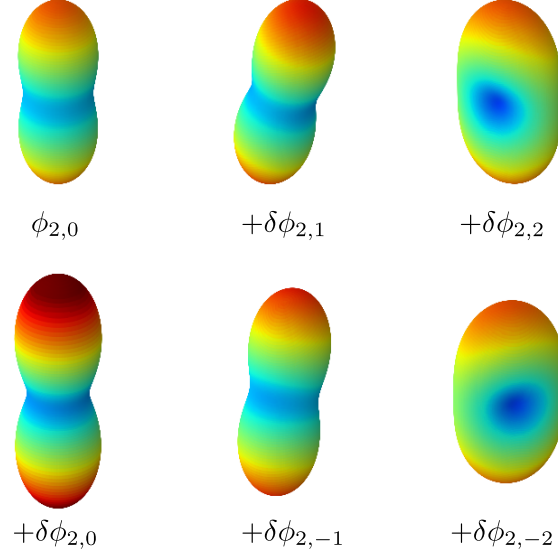


FIG. 6. Distortions of the local orientation probability due to changes in the field strength at various m values. If a small spinner (e.g small molecule) is placed inside the field ϕ then the probability distribution of the orientation of the spinner will go as $\propto \exp(a' \sum_m \phi_{2,m} Y_{2,m}(\vec{u}))$ where a' depends on the magnitude of the spinner. In the above plots the radius in each direction is proportional to the probability that a molecule will point in that direction when it is subject to a field of the form $\phi_{0,0}$ and for various deviations away from $\phi_{0,0}$.

allowing us to write the Fourier representation of bend, twist, and splay as

$$(\hat{n} \cdot \nabla \times \hat{n})^2 = \left(\frac{k_x \tilde{\phi}_{2,-1} - k_y \tilde{\phi}_{2,1}}{\phi_{0,0} \sqrt{3} c_1} \right)^2 \quad (107)$$

$$(\hat{n} \times \nabla \times \hat{n})^2 = \frac{(k_z \tilde{\phi}_{2,1})^2 + (k_z \tilde{\phi}_{2,-1})^2}{(\phi_{0,0} \sqrt{3} c_1)^2} \quad (108)$$

$$(\nabla \cdot \hat{n})^2 = \left(\frac{k_x \tilde{\phi}_{2,1} + k_y \tilde{\phi}_{2,-1}}{\phi_{0,0} \sqrt{3} c_1} \right)^2 \quad (109)$$

Using

$$\kappa_{1,m} = \sqrt{\frac{4\pi}{3}} \begin{cases} k_y & m = -1 \\ k_z & m = 0 \\ k_x & m = 1 \end{cases} \quad (110)$$

and $\phi_{0,0} c_1 = \langle \phi_{2,0} \rangle^{MF}$ we get

$$(\hat{n} \cdot \nabla \times \hat{n})^2 = \frac{(\kappa_{1,1} \tilde{\phi}_{2,-1} - \kappa_{1,-1} \tilde{\phi}_{2,1})^2}{4\pi (\langle \phi_{2,0} \rangle^{MF})^2} \quad (111)$$

$$(\hat{n} \times \nabla \times \hat{n})^2 = \frac{(\kappa_{1,0} \tilde{\phi}_{2,1})^2 + (\kappa_{1,0} \tilde{\phi}_{2,-1})^2}{4\pi (\langle \phi_{2,0} \rangle^{MF})^2} \quad (112)$$

$$(\nabla \cdot \hat{n})^2 = \frac{\left(\kappa_{1,1}\tilde{\phi}_{2,1} + \kappa_{1,-1}\tilde{\phi}_{2,-1}\right)^2}{4\pi \left(\langle\phi_{2,0}\rangle^{MF}\right)^2} \quad (113)$$

Equation 1 can be written in matrix form as

$$E_{Frank} = \frac{1}{2} \left(\langle\phi_{2,0}\rangle^{MF}\right)^{-2} \frac{1}{4\pi} (\vec{\kappa}\vec{\phi}) \cdot \begin{bmatrix} K_{splay} & 0 & 0 & 0 & 0 & B \\ 0 & K_{twist} & 0 & 0 & A & 0 \\ 0 & 0 & K_{bend} & 0 & 0 & 0 \\ 0 & 0 & 0 & K_{bend} & 0 & 0 \\ 0 & A & 0 & 0 & K_{twist} & 0 \\ B & 0 & 0 & 0 & 0 & K_{splay} \end{bmatrix} \cdot (\vec{\kappa}\vec{\phi}) \quad (114)$$

where $A + B = K_{splay} - K_{twist}$ and

$$(\vec{\kappa}\vec{\phi}) = [\kappa_{1,-1}\tilde{\phi}_{2,-1} \quad \kappa_{1,-1}\tilde{\phi}_{2,1} \quad \kappa_{1,0}\tilde{\phi}_{2,-1} \quad \kappa_{1,0}\tilde{\phi}_{2,1} \quad \kappa_{1,1}\tilde{\phi}_{2,-1} \quad \kappa_{1,1}\tilde{\phi}_{2,1}] \quad (115)$$

The Frank elastic constants are related to the deformation energy of the system given in equation 86, in that they comprise the portion of the energy that comes from $\tilde{\phi}_{2,\pm 1}$ deformations that are quadratic in κ . The comparison between equations 111-112 and $\delta\tilde{S}^{-1}$ in equation 86 will allow us to write the Frank elastic constants in terms of the microscopic details of the system (e.g. L , A , $\phi_{0,0}$, a , v_p , etc.).

XIV. FRANK ELASTIC CONSTANTS FOR FUZZBALL AND RIGID ROD

Comparing equations 111-112 and 114 to equation 71 we find that the Frank elastic constants for a fuzzball are identical and equal

$$K_{bend}^{FB} = K_{twist}^{FB} = K_{splay}^{FB} = 3\phi_{0,0} \frac{\sigma^2}{v_p} \frac{(M_{0,2}^0)^2}{M_{2,2}^1 M_{0,0}^0} \quad (116)$$

Comparing equations 111-112 and 114 to equation 75 we get the Frank elastic constants for a rigid rod

$$K_{bend}^{RR} = \phi_{0,0} \frac{L}{A} \frac{2\pi}{3} \frac{(M_{0,2}^0)^2}{M_{2,2}^1 M_{2,2}^1 M_{0,0}^0} \left(J_{(1)}^{1,0,1} \cdot M^1 \cdot J_{(1)}^{1,0,1} \right)_{2,2} \quad (117)$$

$$\begin{aligned} K_{twist}^{RR} = & \phi_{0,0} \frac{L}{A} \frac{2\pi}{3} \frac{(M_{0,2}^0)^2}{M_{2,2}^{-1} M_{2,2}^{-1} M_{0,0}^0} \\ & \times \sum_{\mathcal{M} \in \{-2,0\}} \left(J_{(1)}^{-1,1,\mathcal{M}} \cdot M^{\mathcal{M}} \cdot J_{(1)}^{\mathcal{M},1,-1} \right)_{2,2} \end{aligned} \quad (118)$$

$$\begin{aligned} K_{splay}^{RR} = & \phi_{0,0} \frac{L}{A} \frac{2\pi}{3} \frac{(M_{0,2}^0)^2}{M_{2,2}^1 M_{2,2}^1 M_{0,0}^0} \\ & \times \sum_{\mathcal{M} \in \{0,2\}} \left(J_{(1)}^{1,1,\mathcal{M}} \cdot M^{\mathcal{M}} \cdot J_{(1)}^{\mathcal{M},1,1} \right)_{2,2} \end{aligned} \quad (119)$$

XV. FRANK ELASTIC CONSTANTS FOR WLC

Comparing equations 111-112 and 114 to equation 81 we find the dimensionless elastic constants

$$K'_{splay} = \frac{4\pi (B_1)^2 B_4 (1,1,1,1)}{N^2 (B_2(1))^2 B_0} \quad (120)$$

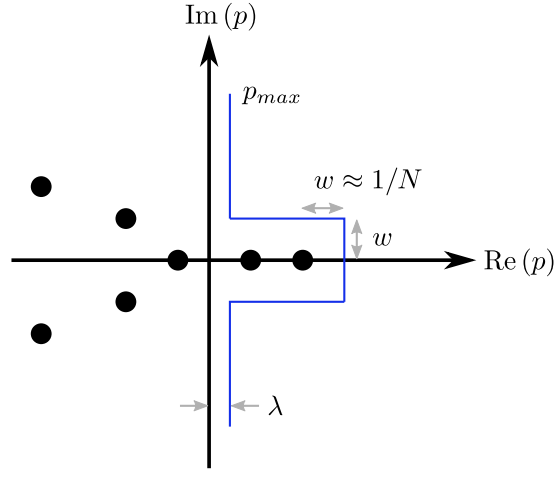


FIG. 7. Diagram of typical path of integration on the complex plane of Laplace variable p . The path goes from bottom to top along the blue lines. Black dots represent typical poll locations. Not drawn to scale, in practice $p_{max} \gg w$.

$$K'_{twist} = \frac{4\pi (B_1)^2 B_4 (-1, -1, 1, 1)}{N^2 (B_2 (-1))^2 B_0} \quad (121)$$

$$K'_{bend} = \frac{4\pi (B_1)^2 B_4 (1, 1, 0, 0)}{N^2 (B_2 (1))^2 B_0} \quad (122)$$

where

$$K' = K \frac{A}{\phi_{0,0} (2\ell_p) N} \quad (123)$$

$$B_0 = \mathcal{L}^{-1} [e_0 \cdot \mathbf{G}^0 \cdot e_0] \quad (124)$$

$$B_1 = \mathcal{L}^{-1} [e_0 \cdot \mathbf{G}^0 \cdot \mathbf{J}_{(2)}^{0,0,0} \cdot \mathbf{G}^0 \cdot e_0] \quad (125)$$

$$B_2(m_1) = \mathcal{L}^{-1} [e_0 \cdot \mathbf{G}^0 \cdot \mathbf{J}_{(2)}^{0,m_1,m_1} \cdot \mathbf{G}^{m_1} \cdot \mathbf{J}_{(2)}^{m_1,m_1,0} \cdot \mathbf{G}^0 \cdot e_0] \quad (126)$$

$$B_4(m_1, m_2, m, m') = \mathcal{L}^{-1} \left[\sum_{\mathcal{M}} e_0 \cdot \mathbf{G}^0 \cdot \mathbf{J}_{(2)}^{0,m_1,m_1} \cdot \mathbf{G}^{m_1} \cdot \mathbf{J}_{(1)}^{m_1,m,\mathcal{M}} \cdot \mathbf{G}^{\mathcal{M}} \cdot \mathbf{J}_{(1)}^{\mathcal{M},m',m_2} \cdot \mathbf{G}^{m_2} \cdot \mathbf{J}_{(2)}^{m_2,m_2,0} \cdot \mathbf{G}^0 \cdot e_0 \right] \quad (127)$$

XVI. NUMERICAL LAPLACE INVERSION

Laplace inversion is accomplished by the numerical integration

$$f(N) = \frac{1}{2\pi i} \int_{\lambda-i\infty}^{\lambda+i\infty} e^{pN} F(p) dp. \quad (128)$$

The complex integration is done along the path in figure 7 where the dots are poles. The position of the first pole is found with binary search using the facts that $\mathbf{G}_{0,0}^0$ changes sign as you go horizontally through the poles and that the first pole is always on the real axis. As the pole moves to the right the $\exp(pN)$ in the integral becomes extremely large. To avoid overflow we can multiply by $\exp(-p_{max}N)$ which will cancel when we take the ratio of two inverse Laplace transforms, as always occurs in this derivation.

Python code to do the inverse Laplace transform and generate the plots in this paper can be found at <https://github.com/SpakowitzLab/wlcsim/tree/master/wlcsim/FrankElastic>. The documentation can be found at <https://wlcsim.readthedocs.io/en/latest/FrankExample.html>.

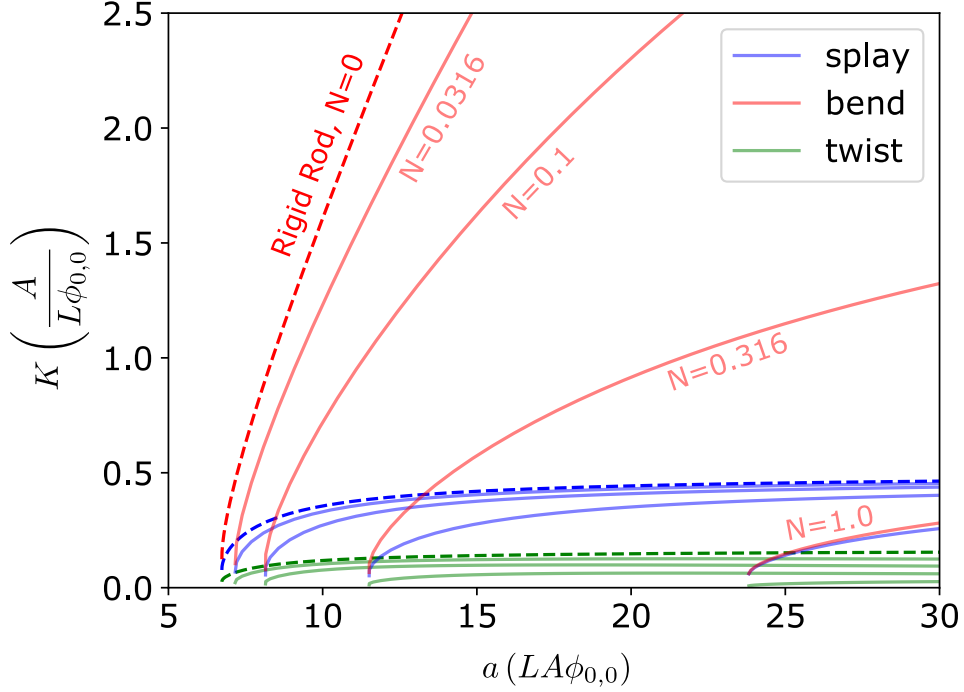


FIG. 8. Frank elastic constants for stiff polymer solutions for stiff chains that are N Kuhn lengths long. Dashed curves are for the rigid rod. For the rigid rod, $K_{\text{splay}} = 3K_{\text{twist}}$.

XVII. RESULTS

The units of the Frank elastic constants are energy times length because they denote energy per unit volume per rate of change of direction squared. To compare the magnitudes of the Frank elastic constants we first nondimensionalize them. Throughout this paper we have dropped the implied energy units of $k_b T$'s, so energy is already dimensionless. For relatively stiff polymers, it makes sense to nondimensionalize K by multiplying it by A/L because L and A are the only relevant length scales for the rigid rod. When nondimensionalizing we also divide the Frank elastic constants by the volume fraction of polymer $\phi_{0,0}$ because denser solutions experience proportionally more aligning field. Figure 8 presents the Frank elastic constants nondimensionalized via $K \left(\frac{A}{L\phi_{0,0}} \right)$. The Maier-Saupe parameter a , which captures the energetic coupling strength of aligning molecules, has units of energy (also in $k_b T$'s) per volume, therefore we nondimensionalize it via $a(LA\phi_{0,0})$. This nondimensionalization is convenient because a rigid rod that is twice as long will experience twice the aligning potential.

In Figure 8 the value of the elastic constants K generally grow with increased Maier-Saupe nematic coupling strength a . The coupling strength drives the formation of a liquid crystal state, so it is natural that higher a could induce higher K and thereby reduce deviations from the perfectly aligned state. Figure 8 shows that liquid crystal solutions of rigid rods and other stiff polymers ($N \ll 1$) have a relatively high bend modulus K_{bend} . Figure 9A shows rigid rods fit poorly into a bending field with their elongated nature inevitably spanning regions of different orientation. In contrast, rods neatly connect together regions of similar orientation making it easy for a solution of rods to twist and splay (see figure 9B and C).

The fundamental difference that leads to K_{bend} being greater than the other K 's is that bend is a change in orientation associated with a displacement in the direction of alignment (see figure 5). This is precisely the direction in which the rod is elongated. To emphasise this point, compare the rod to the fuzball which is equally elongated in all directions and has $K_{\text{twist}}^{FB} = K_{\text{bend}}^{FB} = K_{\text{splay}}^{FB}$.

In figure 8 we see that making a rod-like molecule more flexible (i.e. increasing N) reduces all three elastic constants. The dramatic reduction in K_{bend} reflects the ability of the polymers to bend with a bending field. Increased flexibility also reduces splay and twist constants, but to a lesser extent.

Note that at the lower left corner of figure 8 the elastic constants turn downward and end. They do this because the lower left end of the curve represents the limit of metastability corresponding to the minimum a value in figure 2. At values of a below this cutoff the solution will revert to an isotropic state.

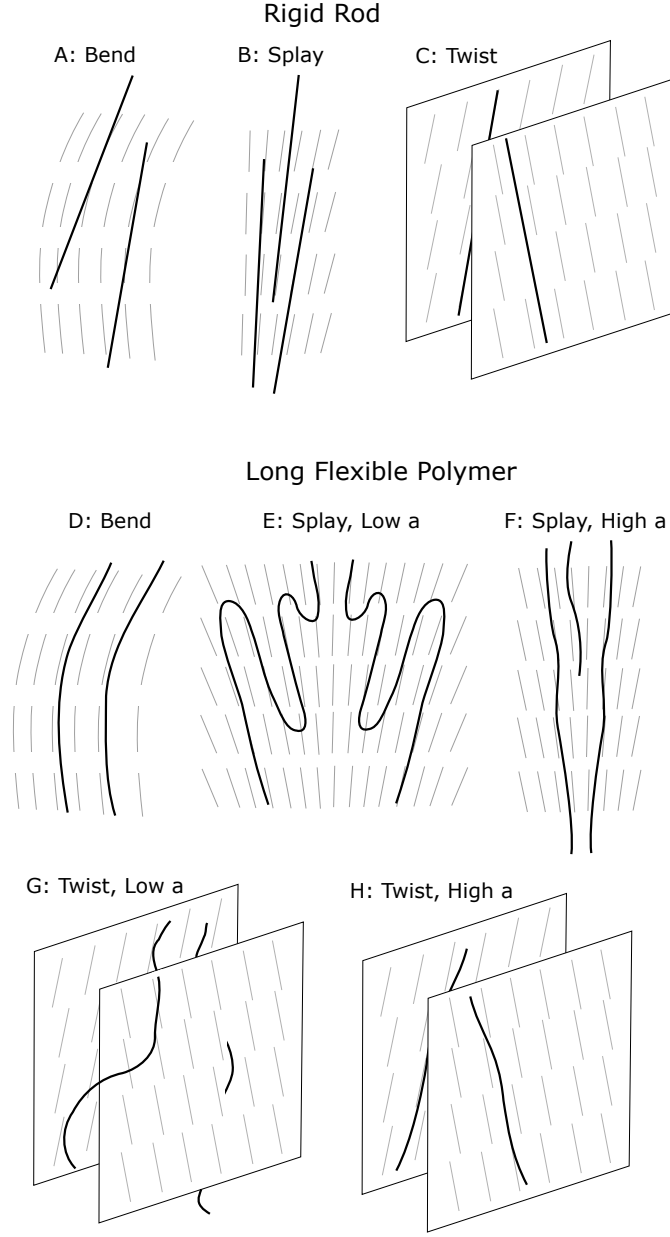


FIG. 9. Schematics providing qualitative arguments for the observed trends in the Frank elastic constants. A-C are for rigid rods or very stiff ($N \ll 1$) polymers. D-H are for long semiflexible polymers ($N \gg 1$).

For relatively flexible polymers it makes sense to nondimensionalize by the Kuhn length, $2\ell_p = L/N$, rather than the length of the entire polymer. In figure 8 the Frank elastic constants decrease with increasing N , in contrast to figure 10 where they increase. The difference between the two is their different nondimensionalization of K . In 8 the polymer length $L = 2\ell_p N$ is held constant so that increasing N makes the chain more flexible and decreases K . In figure 10 the Kuhn length $2\ell_p$ is held constant so that increasing N makes the chain longer and increases K .

Nondimensionalizing by the Kuhn length in figure 10 accentuates the universal behavior of polymers at large N . When comparing a solution of polymers of length $N = 100$ and $N = 200$ but equivalent volume fractions of polymer $\phi_{0,0}$ the solutions look quite similar other than the $N = 200$ solution will have half as many polymer ends. Figure 10 shows that above about $N = 10$ the bend and twist no longer depend on N . Indeed, for relatively flexible ($N \gg 1$) polymers, physical properties (such as the bend and twist moduli) depend much more on the Kuhn length $2\ell_p$ than the total length L . This is consistent with the intuition from figure 9D.

The splay modulus K_{splay} for long polymers is larger and more complex. At low coupling strength splay can be accommodated by hairpins as shown in figure 9E. However, increasing a makes hairpins increasingly energetically

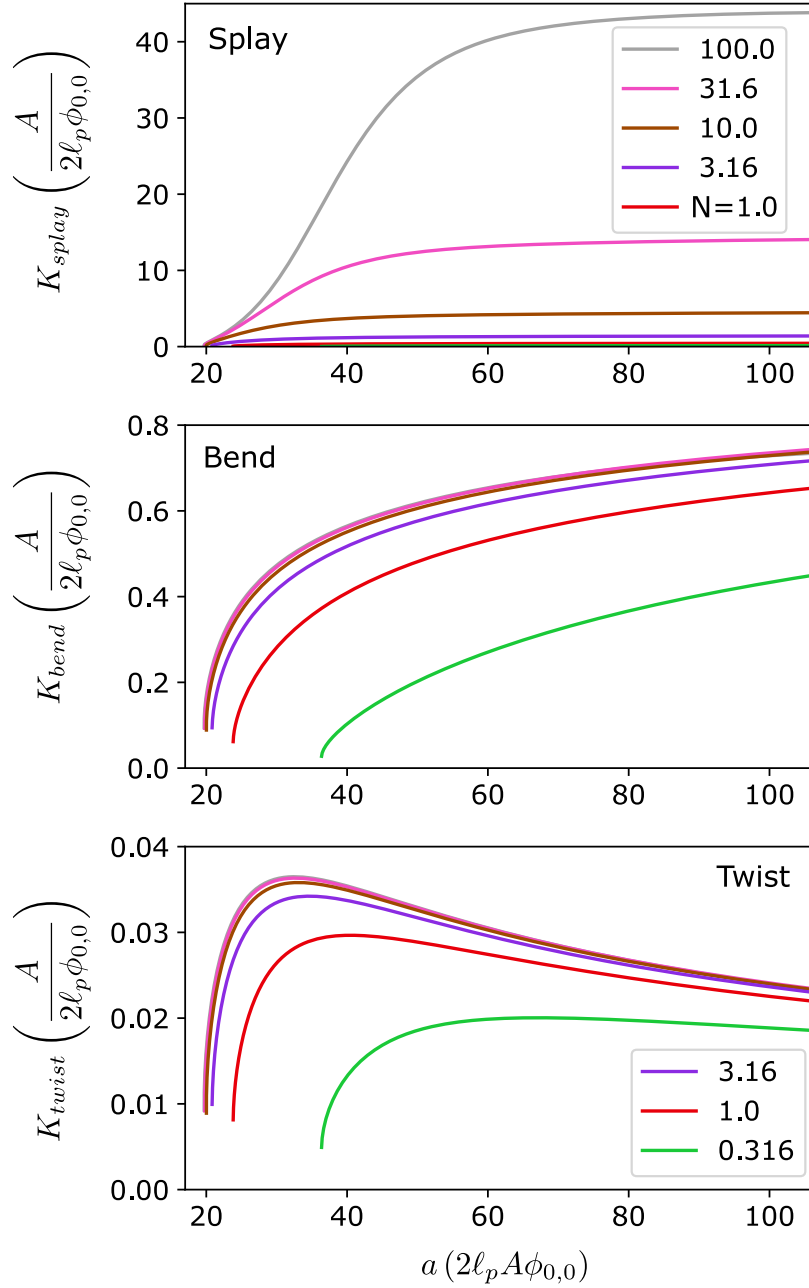


FIG. 10. Frank elastic constants for polymers of different lengths, N , in Kuhn lengths.

unfavorable leading to an exponential growth in the spacing between hairpins and the resulting splay modulus [18]. At sufficiently high a , all hairpins are removed from the chain and the splay is accommodated by chain ends (figure 9F). As the number of chain ends depends on the chain length (at a fixed concentration) rather than a , K_{splay} will plateau at a value that increases with N .

Surprisingly, after initially increasing, the twist modulus K_{twist} moderately decreases with increasing a as shown in figure 10. We justify this by arguing that at low a polymers will mix between twist planes as shown in figure 9G. Each time a polymer mixes between twist planes it introduces stress pulling the orientations of the planes into alignment. As a increases the amount of stress introduced when a polymer mixes between planes increases but the polymers are much less likely to stray from their plane as depicted in 9H. The latter effect apparently overwhelms the former at high a .

The primary trend presented above is that for rigid polymers $N \ll 1$ the $K_{bend} > K_{splay}$ and for long flexible polymers $K_{splay} > K_{bend}$. Naturally, we'd like to know when the crossover between bend and splay occurs. In

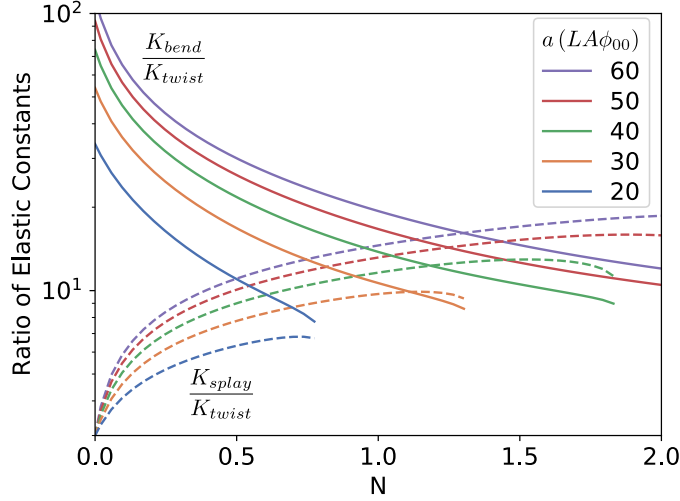


FIG. 11. Ratio of Frank elastic constants for stiff polymers.

figure 11 we plot the ratios of the Frank elastic constants. The crossover where $K_{bend} = K_{splay}$ depends modestly on a and occurs a lengths a little above one Kuhn length. The curves in this figure end when the polymers become flexible to the point where the aligned phase is no longer metastable and spontaneously transforms to the isotropic state. Note that we have nondimensionalized a in this plot by the total polymer length. If we instead had nondimensionalized a by the Kuhn length, the curves would still cross at N values just above one, but the shape of the curves would be different.

XVIII. SUMMARY

We have presented a method for evaluating the size of orientation deformations for nematic solutions of semiflexible polymers. These deformations, described by the Frank elastic constants, are accurately found for a wide range of chain flexibilities and alignment interaction strengths (i.e. persistence length, ℓ_p and Maier-Saupe parameter, a). Our method shows the convenience of combining a previously-derived, stone-fence-diagram-based, exact statistics for the worm-like chain in a quadrupole field [21, 22] with a real-spherical-harmonic orientational density distribution. This method allows us provide both quantitative plots and qualitative explanations for the Frank elastic constants over this range. Here we summarize the features of the Frank elastic constants, some of which have been previously reported.

Below a minimum alignment interaction strength the nematic state will spontaneously degenerate into the isotropic one. That is, the aligned state is not even metastable. This minimum interaction is associated with finite - if small - Frank elastic constants and a large but finite amount of deformation. The following features are for solutions in a stable (or at least metastable) nematic state.

We will divide our results into those for relatively rigid polymers ($L \lesssim \ell_p$) and those for relatively flexible polymers. First, we will make three observations that hold over both ranges. 1) The twist modulus is always smaller than bend and splay moduli. For most polymer solutions K_{twist} is order(s) of magnitude smaller than K_{bend} and K_{splay} . This means that the primary deformation mode of polymer solutions will be twist. 2) At the level of the present theory (no coupling between deformation modes) the Flory Huggins χ parameter does not affect the Frank elastic constants. This means that using a better solvent will not directly[30] affect the Frank elastic constants. 3) Frank elastic constants are inversely proportional to polymer concentration. Higher concentrations lead to more alignment.

For nematic solutions of rigid polymers the Frank elastic constants increase as $L\phi_{0,0}$ where L is the polymer length. That is, increasing polymer length and concentration decreases the expected amount of bend, twist, and splay. Over the range of Maier-Saupe coupling strengths a where liquid crystal alignment can be found, we find $K_{bend} > K_{splay} > K_{twist}$. When coupling strength a is just above the limit of metastability of the nematic phase, then $K_{bend} \approx K_{splay}$ as predicted by [16]. However, with increasing a away from the metastability limit, we find that K_{bend} increases rapidly so that $K_{bend} \gg K_{splay}$. In other words, solutions of long rigid molecules exhibit little bend deformation. Interestingly, for perfectly rigid rods ($N = 0$) we have $K_{splay} = 3K_{twist}$ independent of coupling strength. Furthermore, away from the metastability limit, K_{splay} and $3K_{twist}$ are nearly independent of a , leaving the amount of splay and twist primarily determined by polymer length and concentration.

For nematic solutions of semiflexible and flexible polymers the qualitative elastic behavior differs significantly from

that of rigid polymers. For flexible polymers $K_{splay} > K_{bend}$. The crossover where $K_{bend} = K_{splay}$ occurs at $N \approx 1.25$ with the crossover value increasing modestly with aligning strength a . Unlike solutions of rigid polymers where the elastic constants depended primarily on the polymer length, the elastic constants of semiflexible polymers depend more heavily on the persistence length. In particular, the twist and bend constants, K_{twist} and K_{bend} , grow as $\ell_p \phi_{0,0}$ where ℓ_p is the polymer persistence length. The splay constant K_{splay} grows as $\ell_p \phi_{0,0}$ at low coupling strengths but as $L \phi_{0,0}$ at high coupling strengths.

The dependence of the elastic deformations of flexible polymer solutions have an interesting dependence on coupling strength a . The value of K_{splay} increases quickly with a as hairpins are removed from chains as shown by [18]. The increase flattens off when all the hairpins are removed and splay is accommodated by chain ends. In contrast, after initially increasing, the twist modulus actually *decreases* with increasing coupling strength. Over this range, an increase in the level of alignment of the polymers is associated with an increase in the amount of twist deformation.

Taken together, the elastic deformations depend on the the polymer length, rigidity, and local alignment strength in a varied but predicable fashion. Armed with the knowledge of these dependencies, the reader can both predict and rationally design the liquid crystalline behavior of polymer solutions.

ACKNOWLEDGMENTS

I thank Andrew Spakowitz for is advising during the research and writing of this paper. I thank Ashesh Ghosh for his comments during the editing of this document.

Appendix A: Real Spherical Harmonics

The real spherical harmonics, $Y_{\ell,m}$, are defined in terms the more widely know complex spherical harmonics, Y_l^m , by

$$Y_{\ell,m} = \begin{cases} \frac{i}{\sqrt{2}} (Y_{\ell}^m - Y_{\ell}^{m*}) & m < 0 \\ Y_{\ell}^0 & m = 0 \\ \frac{1}{\sqrt{2}} (Y_{\ell}^{-m} + Y_{\ell}^{-m*}) & m > 0 \end{cases} \quad (\text{A1})$$

and conversely

$$Y_{\ell}^m = \begin{cases} \frac{1}{\sqrt{2}} (Y_{\ell,-m} - iY_{\ell,m}) & m < 0 \\ Y_{\ell,m} & m = 0 \\ \frac{(-1)^m}{\sqrt{2}} (Y_{\ell,m} + iY_{\ell,-m}) & m > 0 \end{cases} \quad (\text{A2})$$

where we note that $Y_{\ell}^{m*} = (-1)^m Y_{\ell}^{-m}$. In particular

$$Y_{0,0} = \frac{1}{\sqrt{4\pi}} \quad (\text{A3})$$

$$Y_{1,m} = \sqrt{\frac{3}{4\pi}} \begin{cases} u_y & m = -1 \\ u_z & m = 0 \\ u_x & m = 1 \end{cases} \quad (\text{A4})$$

$$Y_{2,m}(\vec{u}) = \sqrt{\frac{5}{4\pi}} \begin{cases} \sqrt{3}u_x u_y & m = -2 \\ \sqrt{3}u_y u_z & m = -1 \\ \frac{1}{2}(3u_z^2 - 1) & m = 0 \\ \sqrt{3}u_z u_x & m = 1 \\ \frac{\sqrt{3}}{2}(u_x^2 - u_y^2) & m = 2 \end{cases} \quad (\text{A5})$$

The orthogonality of real spherical harmonics is

$$\int d\vec{u}_i Y_{\ell_1, m_1}(\vec{u}_i) Y_{\ell_2, m_2}(\vec{u}_i) = \delta_{\ell_1, \ell_2} \delta_{m_1, m_2} \quad (\text{A6})$$

A useful property of products of real spherical harmonics is their relation to the Legendre polynomial

$$P_\ell(\vec{u}_1 \cdot \vec{u}_2) = \frac{4\pi}{2\ell+1} \sum_{m=-\ell}^{\ell} Y_{\ell, m}(\vec{u}_1) Y_{\ell, m}(\vec{u}_2) \quad (\text{A7})$$

Furthermore, products of harmonics can be factored into sums of single harmonics

$$Y_{1,0} Y_{\ell, m} = \alpha_{\ell+1}^m Y_{\ell+1, m} + \alpha_\ell^m Y_{\ell-1, m} \quad (\text{A8})$$

$$Y_{2,0} Y_{\ell, m} = \frac{\alpha_{\ell+1}^m \alpha_{\ell+2}^m}{\alpha_2^0} Y_{\ell+2, m} + \frac{\alpha_{\ell+1}^m a_{\ell+1}^m - \alpha_1^0 Y_0^0 + \alpha_\ell^m \alpha_\ell^m}{\alpha_2^0} Y_{\ell, m} + \frac{\alpha_\ell^m \alpha_{\ell-1}^m}{\alpha_2^0} Y_{\ell-2, m} \quad (\text{A9})$$

where

$$\alpha_\ell^m \equiv \sqrt{\frac{3(\ell-m)(\ell+m)}{4\pi(2\ell-1)(2\ell+1)}} \quad (\text{A10})$$

Because it will be used frequently, we will rewrite

$$Y_{2,0} Y_{\ell, m} = A_{\ell+2}^m Y_{\ell+2, m} + \beta_\ell^m Y_{\ell, m} + A_\ell^m Y_{\ell-2, m} \quad (\text{A11})$$

where

$$A_\ell^m \equiv \frac{\alpha_\ell^m \alpha_{\ell-1}^m}{\alpha_2^0}, \quad \beta_\ell^m \equiv \frac{\alpha_{\ell+1}^m a_{\ell+1}^m - \alpha_1^0 Y_{0,0} + \alpha_\ell^m \alpha_\ell^m}{\alpha_2^0} \quad (\text{A12})$$

Furthermore,

$$Y_{1,1} Y_{\ell, m} = \alpha_{\ell+1}^{(+m)} Y_{\ell+1, m+1} f(m+1) - \alpha_{\ell+1}^{(+)}{}^{-m} Y_{\ell+1, m-1} f(m) \\ + \alpha_\ell^{(+)}{}^{m-1} Y_{\ell-1, m-1} f(m) - \alpha_\ell^{(+)}{}^{-m-1} Y_{\ell-1, m+1} f(m+1) \quad (\text{A13})$$

$$Y_{1,-1} Y_{\ell, m} = \alpha_{\ell+1}^{(+)}{}^{-m} \frac{1}{\sqrt{2}} Y_{\ell+1, -m+1} g(m) - \alpha_\ell^{(+)}{}^{m-1} \frac{1}{\sqrt{2}} Y_{\ell-1, -m+1} g(m) \\ + \alpha_{\ell+1}^{(+m)} \frac{1}{\sqrt{2}} Y_{\ell+1, -m-1} h(m) - \alpha_\ell^{(+)}{}^{-m-1} \frac{1}{\sqrt{2}} Y_{\ell-1, -m-1} h(m) \quad (\text{A14})$$

where

$$\alpha_\ell^{(\pm)m} \equiv \sqrt{\frac{3(\ell+m)(\ell+m\pm 1)}{8\pi(2\ell-1)(2\ell+1)}} \quad (\text{A15})$$

$$f(m) = \frac{1}{\sqrt{2}} \cdot \begin{cases} -1 & m < -1 \\ -1 & m = -1 \\ 0 & m = 0 \\ \sqrt{2} & m = 1 \\ 1 & m > 1 \end{cases} \quad \text{and} \quad g(m) = \begin{cases} -1 & m < -1 \\ -1 & m = -1 \\ 0 & m = 0 \\ 0 & m = 1 \\ 1 & m > 1 \end{cases} \quad \text{and} \quad h(m) = \begin{cases} -1 & m < -1 \\ -\sqrt{2} & m = -1 \\ \sqrt{2} & m = 0 \\ 1 & m = 1 \\ 1 & m > 1 \end{cases} \quad (\text{A16})$$

Furthermore

$$Y_{2,\pm 1} Y_{\ell, 0} = \frac{\alpha_{\ell+1}^{(+0)} \alpha_{\ell+2}^1}{\alpha_2^1} Y_{\ell+2, \pm 1} + \frac{\alpha_{\ell+1}^{(+0)} \alpha_{\ell+1}^1 - \alpha_\ell^{(-0)} \alpha_\ell^1}{\alpha_2^1} Y_{\ell, \pm 1} - \frac{\alpha_\ell^{(-0)} \alpha_{\ell-1}^1}{\alpha_2^1} Y_{\ell-2, \pm 1} \quad (\text{A17})$$

$$Y_{2,\pm 2} Y_{\ell, 0} = \frac{\alpha_{\ell+1}^{(+0)} \alpha_{\ell+2}^{(+1)}}{\alpha_2^{(+1)}} Y_{\ell+2, \pm 2} - \frac{\alpha_{\ell+1}^{(+0)} \alpha_{\ell+1}^{(-1)} + \alpha_\ell^{(-0)} \alpha_\ell^{(+1)}}{\alpha_2^{(+1)}} Y_{\ell, \pm 2} + \frac{\alpha_\ell^{(-0)} \alpha_{\ell-1}^{(-1)}}{\alpha_2^{(+1)}} Y_{\ell-2, \pm 2} \quad (\text{A18})$$

At several points throughout this derivation we use the product of three real spherical harmonics combined in matrix form

$$\left(\mathbf{J}_{(\ell)}^{m,m',m''}\right)_{\ell_1,\ell_2} \equiv \int d\vec{u} Y_{\ell_1,m}(\vec{u}) Y_{\ell,m'}(\vec{u}) Y_{\ell_2,m''}(\vec{u}) \quad (\text{A19})$$

The elements of the matrix are mostly zero except a few diagonals which follow from the products above and the orthogonality property. The selection rules for real spherical harmonics differ from that of the complex version. The selection rules dictate that $\mathbf{J}_{(\ell)}^{m,m',m''} = 0$ unless $m + m' - m'' = 0$ or $m - m' + m'' = 0$ or $-m + m' + m'' = 0$.

Appendix B: Fourier Transform Conventions

We use the Fourier transform convention

$$\tilde{f}(\vec{k}) = \frac{1}{(2\pi)^{3/2}} \int d\vec{r} \exp(i\vec{k} \cdot \vec{r}) f(\vec{r}) \quad (\text{B1})$$

and

$$f(\vec{r}) = \frac{1}{(2\pi)^{3/2}} \int d\vec{k} \exp(-i\vec{k} \cdot \vec{r}) \tilde{f}(\vec{k}) \quad (\text{B2})$$

When we extend the summation notation to integrate over \vec{k} rather than \vec{r} it has the effect of reversing the latter \vec{k} . For real functions A and B

$$\begin{aligned} \tilde{A}_1 \tilde{B}_1 &\equiv \sum_{\ell=0}^{\infty} \sum_{m=-\ell}^{\ell} \int d\vec{k} A_{\ell}^m(\vec{k}) B_{\ell}^{m*}(\vec{k}) \\ &= \sum_{\ell=0}^{\infty} \sum_{m=-\ell}^{\ell} \int d\vec{k} A_{\ell}^m(\vec{k}) B_{\ell}^m(-\vec{k}) \end{aligned} \quad (\text{B3})$$

which, along with $\tilde{S}_{12}\tilde{\mathbb{I}}_{23} = \tilde{S}_{13}$, implies that the identity is $\tilde{\mathbb{I}}_{12} = \delta_{\ell_1,\ell_2} \delta_{m_1,m_2} \delta(\vec{k}_1 + \vec{k}_2)$. By plugging B2 into $A_1 B_1$ we find that

$$\begin{aligned} A_1 B_1 &= \frac{1}{(2\pi)^3} \int d\vec{k} \int d\vec{k}' \tilde{A}(\vec{k}) \tilde{B}^*(\vec{k}') \int d\vec{r} e^{-i(\vec{k}-\vec{k}') \cdot \vec{r}} \\ &= \int d\vec{k} \int d\vec{k}' \tilde{A}(\vec{k}) \tilde{B}^*(\vec{k}') \delta(\vec{k} - \vec{k}') \\ &= \tilde{A}_1 \tilde{B}_1 \end{aligned} \quad (\text{B4})$$

Of particular interest to this paper is the forier transform of a derivative squared. To this end we prove equation 106

$$\int dx \left(\frac{\partial}{\partial x} \phi \right)^2 = \int dx \left(\frac{1}{\sqrt{2\pi}} \frac{\partial}{\partial x} \int e^{-ikx} \tilde{f}(k) dk \right)^2 \quad (\text{B5})$$

$$= \int dx \left(\frac{1}{\sqrt{2\pi}} \int (-ik) e^{-ikx} \tilde{f}(k) dk \right)^2 \quad (\text{B6})$$

$$= \int dk_1 \int dk_2 (-ik_1) (-ik_2) \tilde{f}(k_1) \tilde{f}(k_2) \times \frac{1}{2\pi} \int dx e^{-i(k_1+k_2)x} \quad (\text{B7})$$

$$= - \int dk_1 \int dk_2 k_1 k_2 \tilde{f}(k_1) \tilde{f}(k_2) \delta(k_1 + k_2) \quad (\text{B8})$$

$$= \int k^2 \tilde{f}(k) \tilde{f}(-k) dk \quad (\text{B9})$$

All interactions discussed in this paper are assumed to be translationally invariant (assumption 7) meaning that for some interaction $S(\vec{x}_1, \vec{x}_2) = S(\vec{x}_1 + \vec{x}_0, \vec{x}_2 + \vec{x}_0)$ for all \vec{x}_0 . Taking the Fourier transform

$$\tilde{S}(\vec{k}_1, \vec{k}_2) = \frac{1}{(2\pi)^3} \int_{-\infty}^{\infty} d\vec{x}_2 d\vec{x}_1 e^{i\vec{k}_1 \cdot \vec{x}_1 + i\vec{k}_2 \cdot \vec{x}_2} S(\vec{x}_1, \vec{x}_2) \quad (\text{B10})$$

because of the infinite extent of the system we can do a change of integration variables $\vec{x}_3 = \vec{x}_1 + \vec{x}_0$

$$\begin{aligned} \tilde{S}(\vec{k}_1, \vec{k}_2) &= \frac{1}{(2\pi)^3} \int_{-\infty}^{\infty} d\vec{x}_2 d\vec{x}_3 e^{i\vec{k}_1 \cdot (\vec{x}_3 - \vec{x}_0) + i\vec{k}_2 \cdot \vec{x}_2} \\ &\quad \times S(\vec{x}_3 - \vec{x}_0, \vec{x}_2) \end{aligned} \quad (\text{B11})$$

using the definition of translation invariance $S(\vec{x}_3 - \vec{x}_0, \vec{x}_2) = S(\vec{x}_3, \vec{x}_2 + \vec{x}_0)$ and setting $\vec{x}_0 = -\vec{x}_2$ yields

$$\begin{aligned} \tilde{S}(\vec{k}_1, \vec{k}_2) &= \frac{1}{(2\pi)^3} \int_{-\infty}^{\infty} d\vec{x}_2 d\vec{x}_3 e^{i\vec{k}_1 \cdot (\vec{x}_3) + i(\vec{k}_1 + \vec{k}_2) \cdot \vec{x}_2} \\ &\quad \times S(\vec{x}_3, 0) \end{aligned} \quad (\text{B12})$$

Recognizing the delta function $(2\pi)^3 \delta(\vec{k}_1 + \vec{k}_2) = \int_{-\infty}^{\infty} d\vec{x}_2 \exp(i(\vec{k}_1 + \vec{k}_2) \cdot \vec{x}_2)$ and defining $\tilde{S}(\vec{k}) = \int_{-\infty}^{\infty} d\vec{x} \exp(i\vec{k} \cdot \vec{x}) S(\vec{x}, 0)$ we have

$$\tilde{S}(\vec{k}_1, \vec{k}_2) = \tilde{S}(\vec{k}_1) \delta(\vec{k}_1 + \vec{k}_2) \quad (\text{B13})$$

Being diagonal with respect to \vec{k} makes \tilde{S} easy to invert. We define the inverse by $\tilde{S} \cdot \tilde{S}^{-1} \equiv \mathbb{I}$ which written out implies

$$\tilde{S}^{-1}(k_1, k_3) = \frac{\delta(\vec{k}_1 + \vec{k}_2)}{\tilde{S}(\vec{k}_1)} \quad (\text{B14})$$

Note that if \tilde{S} contains ℓ and m indices, it still needs to be inverted with respect them in the normal way.

Appendix C: Inverting S

As the deformation energy 86 requires the inverse of S , we will take a moment to discuss how to take the inverse of a power series of matrices. The derivative of an inverse can be calculated by differentiating the identity $\partial I = 0 = \partial(SS^{-1}) = S\partial(S^{-1}) + (\partial S)S^{-1}$ which gives

$$\partial(S^{-1}) = -S^{-1}(\partial S)S^{-1} \quad (\text{C1})$$

$$\begin{aligned} \frac{\partial}{\partial \kappa_1} \frac{\partial}{\partial \kappa_2} (S^{-1}) &= S^{-1} \left(\frac{\partial}{\partial \kappa_1} S \right) S^{-1} \left(\frac{\partial}{\partial \kappa_2} S \right) S^{-1} \\ &\quad + S^{-1} \left(\frac{\partial}{\partial \kappa_2} S \right) S^{-1} \left(\frac{\partial}{\partial \kappa_1} S \right) S^{-1} \\ &\quad - S^{-1} \left(\frac{\partial}{\partial \kappa_2} \frac{\partial}{\partial \kappa_1} S \right) S^{-1} \end{aligned} \quad (\text{C2})$$

$$S^{-1}(\kappa) = S^{-1}|_{\kappa=0} + \frac{\partial}{\partial \kappa} S^{-1}(\kappa) \Big|_{\kappa=0} \kappa + \frac{1}{2} \frac{\partial^2}{\partial \kappa^2} S^{-1}(\kappa) \Big|_{\kappa=0} \kappa^2 \quad (\text{C3})$$

In other words, if we have a Taylor expansion

$$S(\kappa) = S + S_{\kappa\kappa}(\kappa^2) \quad (\text{C4})$$

then

$$S^{-1}(\kappa) = S^{-1} - S^{-1} S_{\kappa\kappa}(\kappa^2) S^{-1}. \quad (\text{C5})$$

Appendix D: List of Variables and Notation

Variables

- A – polymer cross sectional area (also matrix element in equation 114)
- A_ℓ^m – defined in equations A12
- a – Maier-Saupe parameter
- B – a particular matrix element in equation 114
- $B_{(n)}$ – products of propagators defined and used in section XV
- c_i – degree of alignment, expressed as s_i in [29], see equation 89
- e_0 – unit vector for $\ell = 0$, i.e. $[1, 0, 0, \dots, 0]$
- \vec{e}_i – eigenvector of alignment matrix, see equation 88
- E_{FH} – Flory-Huggins Separation energy
- E_{Frank} – Frank elastic energy
- E_{MS} – Maier-Saupe alignment energy
- E_{poly} – polymer bending energy
- f – used to denote arbitrary function
- FB – super script indicating fuzzball system
- G – propagator for wormlike chain in aligning field (not normalized!), see equation 37
- G_o – propagator for wormlike chain given in equation 35
- $G_{\ell_0 \ell_f}^m$ – \check{G} coefficient, see equation 51
- \mathbf{G}^m – \check{G} coefficient matrix representation $(\mathbf{G}^m)_{\ell_1, \ell_2} \equiv G_{\ell_1, \ell_2}^m$
- h – short for $\lim_{k \rightarrow 0} S'_{02}00$, see equation 85
- I – 3x3 identity matrix
- \mathbb{I}_{12} – the identity in the space defined by our summation notation
- i – $\sqrt{-1}$ or index depending on context
- j – polymer or monomer index
- \mathbf{J} – product of three spherical harmonics defined in A19
- \vec{k} – Fourier conjugate of position
- K – Frank elastic content.
- K' – Nondimensionalized Frank elastic content.
- L – path length of polymer
- $\mathcal{L}[\dots]$ – Laplace transform $N \rightarrow p$
- $\mathcal{L}^{-1}[\dots](N)$ – Inverse Laplace transform $N \leftarrow p$
- ℓ – angular momentum eigenvalue
- ℓ_p – persistence length of the polymer when placed in isotropic solution
- $\mathbf{M}_{\ell_1, \ell_2}^m$ – rigid rod/fuzzball matrix, see equation 27
- M – 3x3 alignment matrix defined by equation 87
- m – z-component of angular momentum eigenvalue
- \mathcal{M} – m value in particular summations.
- N – polymer length in Kuhn lengths, $N \equiv L / (2\ell_p)$
- n – order in γ expansion, see equation 40
- \vec{n} – nematic director defined in equation 88
- n_p – number of polymers
- p – Laplace transform variable of N
- P – Legendre polynomial
- P – probability propagator, see equation 38
- P_ℓ – shorthand for $p + \ell(\ell + 1)$
- Q – traceless alignment matrix $M - \frac{1}{3}I$
- RR – super script indicating rigid rod
- $\vec{r}_j(s)$ – position of point s along polymer j
- \vec{r}_1 – shorthand for $\vec{r}(s_1)$
- \vec{r} – arbitrary position in space
- s – path length along polymer
- S_{12} – two point correlation (single polymer structure factor), see equation 65
- t – short for $\lim_{k \rightarrow 0} S'_{00}00$, see equation 85
- $\vec{u}_j(s)$ orientation unit vector $\frac{\partial \vec{r}_j(s)}{\partial s}$ for polymer j at path length s
- \vec{u}_1 – shorthand for $\vec{u}(s_1)$

\vec{u}_1 – arbitrary unit vector
 \mathcal{V} – volume of space (assumed to be large)
 V_{12} – interaction potential defined in equation 11
 v – rotational term in equation 68
 v_p – volume of one polymer, rod, or fuzzball
 W – field conjugate to ϕ , similar to chemical potential, see equation 16
 $W_\ell^{(\pm)m}$ – see equation 50
 $W_\ell^{(+m)}$ – see equation 48
 $W_\ell^{(-m)}$ – see equation 49
 w – distance to avoid pole by inverse Laplace transform, see section XVI
 x – short for $\lim_{k \rightarrow 0} S'_{22}00$, see equation 85
 \hat{x} – Cartesian unit vector
 y – short for $\lim_{k \rightarrow 0} S'_{22}\pm 1 \pm 1$, see equation 85
 \hat{y} – Cartesian unit vector
 Y_l^m – real spherical harmonic. We use the normalization $\int d\vec{u} Y_l^m(\vec{u}) Y_{l'}^{*m'}(\vec{u}) = \delta_{\ell,\ell'} \delta_{m,m'}$
 \hat{z} – Cartesian unit vector
 Z – multi-polymer partition function
 z – short for $\lim_{k \rightarrow 0} S'_{22}\pm 2 \pm 2$, see equation 85
 z_p – single polymer partition function, see equation 19
 α_ℓ^m – raising symbol, defined in equation A10
 $\alpha_\ell^{(\pm)m}$ – raising symbol with change in m , defined in equation A15
 β_ℓ^m – defined in equations A12
 Γ_{12} – the quadratic order fluctuation coefficient, see 66
 γ – aligning field strength
 ∇ – derivative vector $\hat{x}\partial_x + \hat{y}\partial_y + \hat{z}\partial_z$
 ΔV – coarse-graining volume element
 $\delta(\dots)$ – delta function or product of delta function at every point in space as in equation 16
 $\delta\phi$ – fluctuations in ϕ from it's mean field value
 δW – fluctuations in W from it's mean field value
 δS_{12} – first term in 65
 κ_1^m – spherical representation of \vec{k} as defined in 78
 λ – real offset in numerical inverse Laplace transform see section XVI
 ρ – spatial term in equation 68
 σ – standard deviation of a fuzzball
 ϕ – smooth field approximately equal to $\hat{\phi}$
 $\hat{\phi}_l^m(\vec{r})$ – polymer position and orientation field defined in equation 7
 χ – Flory-Huggins interaction parameter

Notation

$\int \mathcal{D}[\vec{r}_j(s)]$ – functional integral of positions of polymers defined in equation 9
 $\int \mathcal{D}W = \prod_{\vec{r}} (\int dW(\vec{r}))$ – functional integral of W over all space
 $\int d\vec{u}$ – Integral over surface of ball $\int \sin(\theta) d\theta d\phi$
 \propto – proportional to
 \equiv – definition
 $\vec{u} \otimes \vec{v}$ – outer product matrix $(\vec{u} \otimes \vec{v})_{i,j} = u_i v_j$
 $A_1 B_1 \equiv \sum_{\ell=0}^{\infty} \sum_{m=-\ell}^{\ell} \int d\vec{r} A_\ell^m(\vec{r}) B_\ell^{m*}(\vec{r})$ – extended summation notation
 $f * g$ – convolution $f * g = \int_0^t d\tau f(\tau) g(t - \tau)$
 $G(\vec{u}|\vec{u}_0; L)$ – distribution $G(\vec{u})$ given \vec{u}_0 for polymer of length L
 $\dots^{(1)}$ – superscript denoting single polymer
 \dots^{MF} – superscript denoting mean field
 $\langle \dots \rangle^{MF}$ – mean field expectation value as in equation 21
 $\langle \dots \rangle_o$ – expectation value for free chain (no applied field) with fixed end orientations, see example 36
 \dots – indicates Laplace transform $N \rightarrow p$
 $\tilde{\dots}$ – indicates Fourier transform $\vec{r} \rightarrow \vec{k}$
 $\vec{\dots}$ – Euclidean vector in 3 dimensions

Stone Fence symbols

All symbols are assumed to start from ℓ on the left.

$$\begin{aligned}
\bullet &= 1/P_\ell \\
\text{---} &= \gamma\beta_\ell^m \\
\diagdown &= \gamma A_\ell^m \\
\diagup &= \gamma A_{\ell+2}^m \\
\bullet \text{---} \bullet &= 1/(P_\ell - \gamma\beta_\ell^m) \\
\bullet \text{---} \updownarrow \bullet &= W_\ell^{(+)-m} \\
\bullet \text{---} \downarrow \up \bullet &= W_\ell^{(-)-m} \\
\circ \text{---} \bullet &= (P_\ell - \gamma\beta_\ell^m) W_\ell^{(+)-m} - 1 \\
\circ \text{---} \bullet &= (P_\ell - \gamma\beta_\ell^m) W_\ell^{(-)-m} - 1 \\
\bullet \text{---} \updownarrow \bullet &= W_\ell^{(\pm)-m}
\end{aligned}$$

- [1] J. V. Selinger, Interpretation of saddle-splay and the Oseen-Frank free energy in liquid crystals, *Liquid Crystals Reviews* **6**, 129 (2018), arXiv: 1901.06306.
- [2] P. E. Rudnicki, Q. MacPherson, L. Balhorn, B. Feng, J. Qin, A. Salleo, and A. J. Spakowitz, Impact of Liquid-Crystalline Chain Alignment on Charge Transport in Conducting Polymers, *Macromolecules* 10.1021/acs.macromol.9b01729 (2019).
- [3] D. Svenšek, G. Veble, and R. Podgornik, Confined nematic polymers: Order and packing in a nematic drop, *Physical Review E* **82**, 011708 (2010), publisher: American Physical Society.
- [4] A. R. Khokhlov and A. N. Semenov, Liquid-crystalline ordering in the solution of long persistent chains, *Physica A: Statistical Mechanics and its Applications* **108**, 546 (1981).
- [5] A. R. Khokhlov and A. N. Semenov, Liquid-crystalline ordering in the solution of partially flexible macromolecules, *Physica A: Statistical Mechanics and its Applications* **112**, 605 (1982).
- [6] A. R. Khokhlov and A. N. Semenov, Influence of external field on the liquid-crystalline ordering in the solutions of stiff-chain macromolecules, *Macromolecules* **15**, 1272 (1982), publisher: American Chemical Society.
- [7] A. R. Khokhlov and A. N. Semenov, On the theory of liquid-crystalline ordering of polymer chains with limited flexibility, *Journal of Statistical Physics* **38**, 161 (1985).
- [8] A. R. Khokhlov and A. N. Semenov, Theory of nematic ordering in the melts of macromolecules with different flexibility mechanisms, *Macromolecules* **19**, 373 (1986), publisher: American Chemical Society.
- [9] A. N. Semenov and A. R. Khokhlov, Statistical physics of liquid-crystalline polymers, *Soviet Physics Uspekhi* **31**, 988 (1988), publisher: IOP Publishing.
- [10] A. J. Liu and G. H. Fredrickson, Free energy functionals for semiflexible polymer solutions and blends, *Macromolecules* **26**, 2817 (1993).
- [11] A. J. Spakowitz and Z.-G. Wang, Semiflexible polymer solutions. I. Phase behavior and single-chain statistics, *The Journal of Chemical Physics* **119**, 13113 (2003).
- [12] J. P. Straley, Frank Elastic Constants of the Hard-Rod Liquid Crystal, *Physical Review A* **8**, 2181 (1973), publisher: American Physical Society.
- [13] S. Lee and R. B. Meyer, Computations of the phase equilibrium, elastic constants, and viscosities of a hard-rod nematic liquid crystal, *The Journal of Chemical Physics* **84**, 3443 (1986), publisher: American Institute of Physics.
- [14] G. Marrucci and F. Greco, The Elastic Constants of Maier-Saupe Rodlike Molecule Nematics, *Molecular Crystals and Liquid Crystals* **206**, 17 (1991), publisher: Taylor & Francis _eprint: <https://doi.org/10.1080/00268949108037714>.
- [15] T. Odijk, Elastic constants of nematic solutions of rod-like and semi-flexible polymers, *Liquid Crystals* **1**, 553 (1986), publisher: Taylor & Francis _eprint: <https://doi.org/10.1080/02678298608086279>.
- [16] T. Shimada, M. Doi, and K. Okano, Coefficiens of Gradient Terms in Landau-de Gennes Free Energy Expansion for Polymeric Liquid Crystals, *Journal of the Physical Society of Japan* **57**, 2432 (1988), publisher: The Physical Society of Japan.
- [17] P. L. Doussal and D. R. Nelson, Statistical Mechanics of Directed Polymer Melts, *Europhysics Letters (EPL)* **15**, 161 (1991), publisher: IOP Publishing.
- [18] R. G. Petschek and E. M. Terentjev, Molecular-statistical theory for curvature elasticity of thermotropic main-chain-polymer liquid crystals, *Physical Review A* **45**, 930 (1992), publisher: American Physical Society.
- [19] T. Sato and A. Teramoto, On the Frank Elastic Constants of Lyotropic Polymer Liquid Crystals, *Macromolecules* **29**, 4107 (1996), publisher: American Chemical Society.

- [20] It appears that this approximation roughly corresponds to including only the leading pole in the complex integral we perform in section XVI.
- [21] A. J. Spakowitz and Z.-G. Wang, Exact Results for a Semiflexible Polymer Chain in an Aligning Field, *Macromolecules* **37**, 5814 (2004).
- [22] A. J. Spakowitz and Z.-G. Wang, End-to-end distance vector distribution with fixed end orientations for the wormlike chain model, *Physical Review. E, Statistical, Nonlinear, and Soft Matter Physics* **72**, 041802 (2005).
- [23] R. G. Priest, Theory of the Frank Elastic Constants of Nematic Liquid Crystals, *Physical Review A* **7**, 720 (1973).
- [24] Without the factor of 1/2 the E_{MS} would have a 2/3 rather than a 1/3 per the customary definition of a .
- [25] H. Yamakawa, *Helical Wormlike Chains in Polymer Solutions* (Springer-Verlag, Berlin Heidelberg, 1997).
- [26] L. Leibler, Theory of microphase separation in block copolymers, *Macromolecules* **13**, 1602 (1980).
- [27] S. Mao, Q. Macpherson, S. He, E. Coletta, and A. Spakowitz, Impact of conformational and chemical correlations on microphase segregation in random copolymers, *Macromolecules* **49**, 10.1021/acs.macromol.5b02639 (2016).
- [28] For WLCs the Kuhn length is twice the persistence length.
- [29] S. Turzi, *Distortion-induced effects in nematic liquid crystals*, Ph.D. thesis, Politecnico di Milano, Milan, Italy (2007).
- [30] A better solvent could effect behavior on shorter length scales which could renormalize into a different Maier-Saupe parameter on longer length scales and thereby indirectly effect the Frank elastic constants. We have also assumed that all solvents are good enough to dissolve the polymers.